International Journal of Heat and Mass Transfer 164 (2021) 120587

Contents lists available at ScienceDirect

International Journal of Heat and Mass Transfer

journal homepage: www.elsevier.com/locate/hmt

Effect of aspect ratio on flow boiling characteristics in microchannels

Ali H. Al-Zaidi[a], Mohamed M. Mahmoud[b], Tassos G. Karayiannis[c,*]

[a] University of Misan, Al-Amarah, 62001, Iraq
[b] Faculty of Engineering, Zagazig University, Zagazig, 44519, Egypt
[c] Department of Mechanical and Aerospace Engineering, Brunel University London, Uxbridge, UB8 3PH, United Kingdom

ARTICLE INFO

Article history:
Received 24 April 2020
Revised 25 July 2020
Accepted 9 October 2020

Keywords:
Microchannel
Electronics cooling
Flow boiling
Channel aspect ratio
Flow patterns
Boiling instability
Heat transfer
Pressure drop

ABSTRACT

The effect of channel aspect ratio on flow boiling characteristics (flow patterns, heat transfer and pressure drop) of HFE-7100 in copper multi-microchannel heat sinks was investigated experimentally. Three heat sinks with base area 500 mm^2, channel hydraulic diameter 0.46 mm and channel aspect ratio (ratio of channel width to channel height) of 0.5, 1.0 and 2.0 were tested. The average surface roughness of the channel bottom surface was nearly the same in the three heat sinks and the measured values were 0.271, 0.286 and 0.304 μm. The local heat transfer rates were determined simultaneously with flow visualisation at mass flux ranging from 50 to 250 kg/m^{2}s, wall heat flux from 9.6 to 191.6 kW/m^2, system pressure of 1 bar and low inlet sub-cooling of 5 K. The results showed that, when the channel aspect ratio increased, the heat transfer coefficient increased, while the flow boiling pressure drop decreased. However, the heat transfer rate calculated using the heat sink base area was higher in the heat sink with the smallest channel aspect ratio, indicating an enhancement due to the largest surface area.

1. Introduction

Flow boiling in microchannel evaporators has the capability of dissipating huge quantities of heat from a small area with nearly uniform surface temperature and low pumping power for a given thermal load. Thus, it is a very promising technique for cooling electronics equipment and other high heat flux devices. A significant number of past papers is available in the literature describing work aimed at understanding fundamental issues that relate to flow boiling in small to micro passages, including the prevailing flow patterns, the heat transfer mechanisms, the effect of fluid properties and channel dimensions and geometry. The present paper focuses on studying the effect of channel aspect ratio (ratio of channel width to channel height) on flow boiling characteristics in rectangular microchannels. Thus, the effect of this parameter on flow boiling characteristics is reviewed and discussed in the following paragraphs. For a more general review on flow boiling in small to micro tubes and passages the interested reader is referred to references [1-3].

Singh et al. [4] studied flow boiling of water in horizontal single rectangular silicon microchannels having a fixed hydraulic diameter of 0.142 mm, aspect ratio values of 1.23–3.75 and average roughness less than 0.1 μm. They conducted their experiments at 45 K inlet sub-cooling, low input power of 3 W and 3.5 W and mass flow rate of 0.15–0.2 mL/min. They assessed the effect of aspect ratio based on the input power and mass flow rate, rather than heat and mass fluxes, to allow comparison at the same exit vapour quality. Their results indicated that, for a fixed input power and mass flow rate, the two-phase pressure drop decreased to a minimum value with increasing channel aspect ratio then increased with further increase of aspect ratio. The minimum pressure drop value was found to occur at channel aspect ratio of 1.56. It is worth mentioning that the tests conducted by Singh et al. [4] were nearly at boiling incipience, i.e. very low vapour quality values. This might not be enough to get a conclusion on the effect of aspect ratio on two phase pressure drop. Additionally, with keeping the input power and mass flow rate fixed, the heat and mass fluxes are not the same in these test sections.

Harirchian and Garimella [5] conducted an experimental investigation of flow boiling heat transfer of FC-77 in horizontal silicon multi-microchannels at 5 K inlet sub-cooling and mass flux range 250–1600 kg/m^{2}s. Seven heat sinks with the same channel depth, i.e. 0.4 mm, and different channel widths ranging from 0.1 to 5.85 mm (aspect ratio range 0.25–14.6) were manufactured

* Address correspondence to: Prof. Tassos G. Karayiannis, Department of Mechanical and Aerospace Engineering, Brunel University London, Uxbridge, Middlesex, UB8 3PH, UK.
E-mail address: tassos.karayiannis@brunel.ac.uk (T.G. Karayiannis).

https://doi.org/10.1016/j.ijheatmasstransfer.2020.120587

Nomenclature

A	Area, [m^2]
b	Distance between thermocouple and channel bottom, [m]
C	Dimensionless correction factor, [-]
cp	Specific heat at constant pressure, [J/kgK]
D_h	Hydraulic diameter, [m]
f	Fanning friction factor, [-]
G	Mass flux, [kg/m^2s]
H	Height, [m]
h	Heat transfer coefficient, [W/m^2K]
$\bar{h}$	Average heat transfer coefficient, [W/m^2K]
i	Specific enthalpy, [J/kg]
i_{lg}	Latent heat of vaporization, [J/kg]
k	Thermal conductivity, [W/mK]
K_{90}	The loss coefficient of the 90° turns, [-]
K_∞	Dimensionless incremental pressure drop number, [-]
L	Length, [m]
L^*	Dimensionless length, [-]
m	Fin parameter, [-]
$\dot{m}$	Mass flow rate, [kg/s]
N	Number of channels, [-]
$\overline{Nu}$	Average Nusselt number, [-]
P	Pressure, [Pa]
q''	Heat flux, [W/m^2]
Ra	Average surface roughness, [μm]
Re	Reynolds number, [-]
v	Specific volume, [m^3/kg]
W	Width, [m]
x	Vapour quality, [-]
Z	Axial distance, [m]

Greek Symbols

α	Area ratio, [-] $\alpha = A_{ht}/A_b$ [in Eq. (17)]
β	Aspect ratio, [-] $\beta = W_{ch}/H_{ch}$
ΔP	Pressure drop, [Pa]
ΔT_{LM}	Log mean temperature difference, [K]
η	Fin efficiency, [-]
ρ	Density, [kg/m^3]
σ	Surface tension, [N/m]
η	Fin efficiency, [-]

Subscript

app	Apparent
b	Base
cu	Copper
ch	Channel
exp	Experimental
f	Fluid
FD	Fully developed
fin	Channel fin
g	Gas or vapour
ht	Heat transfer
i	Inlet
ip	Inlet plenium
l	Liquid
Max	Maximum
meas	Measurment
min	Minimum
o	Outlet
op	Outlet plenium
p	Plenium
sc	Sudden contraction
se	Sudden expansion
sub	Subcooled
th	Thermocouple
tp	Two-phase
w	Wall
wi	Internal wall surface
z	Axial local

and tested. The channel hydraulic diameter was not constant for these heat sinks, i.e. ranged from 0.16 to 0.75 mm, and the average surface roughness of the channel bottom wall ranged from 0.1 to 1.4 μm. It is worth mentioning that their tests were conducted with inlet restriction to supress flow instabilities, i.e. a throttling valve was installed ahead of the test sections. It was found that, at a given wall heat flux, the two-phase pressure drop increased with decreasing channel width (aspect ratio). Additionally, when the heat transfer coefficient was plotted versus the wall heat flux, the effect of channel width (aspect ratio) was insignificant. On the contrary, when the heat transfer coefficient was plotted versus the base heat flux, a clear effect of the channel width (aspect ratio) was detected and the heat transfer coefficient increased with increasing channel width (aspect ratio). Harirchian and Garimella [6] presented results of flow visualization using the same test sections and fluid as in [5] but in the mass flux range of 225–1420 kg/m^2s. They mentioned that bubbly, slug, churn, wispy-annular, and annular flow were captured. The results demonstrated that the flow patterns in the channels with 0.1 mm width was different compared to the flow patterns observed in the channels with larger widths. The differences include the following: (i) Bubbly flow was not observed; instead slug flow appeared immediately after boiling incipience; (ii) In the slug and annular flows, the liquid film is seen to break up at the locations of the nucleating bubbles resulting in a discontinuous liquid film. This resulted in a flow pattern that was altering between annular flow with a smooth liquid film and annular flow with a discontinuous liquid film and (iii) There was no droplet entrainment to the vapour core in the annular flow. It is worth mentioning that bubble nucleation in slug, churn, wispy annular and annular flows was observed. Additionally, slug flow was not observed in the channel of width 5.85 mm due to the high aspect ratio and the alternating churn/wispy-annular flow were distributed side by side along the channel width, i.e. they didn't follow each other along the channel length. Finally, it was concluded that when the channel width increased, bubbly flow replaced slug flow, and the churn/wispy-annular flow replaced the churn/annular flow. Harirchian and Garimella [7] used the same experimental facility and fluid as in [5-6] and examined twelve test sections to study the effect of channel width, depth, aspect ratio, hydraulic diameter and cross sectional area. The channel depth was varied from 0.1 to 0.4 mm, the aspect ratio was varied from 0.27 to 15.55 for cross-sectional area of 0.009–2.201 mm^2, while the hydraulic diameter ranged from 0.096 to 0.707 mm. The bottom wall of the microchannels had an average roughness ranging from 0.1 to 1.4 μm, similar to the work described in [5]. It was concluded that, for channels with cross sectional area $\leq$ 0.037 mm^2 ($D_h \leq$ 0.159 mm), bubbly flow did not exist, while slug and annular flow regimes were dominant. For channels with cross sectional area between 0.037 and 0.089 mm^2 (D_h between 0.159 and 0.291 mm), bubbly, slug and annular flows existed. For channels with cross sectional area $\geq$ 0.144 mm^2 ($D_h \geq$ 0.379 mm), bubbly flow appeared at boiling incipience followed by alternating churn/wispy-annular flows, i.e. no slug flow. The heat transfer results indicated that for channels with cross sectional area $\geq$ 0.089 mm^2,

the heat transfer coefficient was independent of the microchannel size, which was attributed to the dominance of nucleate boiling in these channels. On the contrary, for channels with cross sectional area below this value, the heat transfer coefficient exhibited higher values compared to the larger channels, especially at low to intermediate heat fluxes. Additionally, the pressure drop was found to increase with decreasing channel cross-sectional area for a given mass and heat flux. For channels with a fixed cross sectional area but different aspect ratio, the pressure drop was the same.

Holcomb et al. [8] from the same group as [5-7], studied flow boiling heat transfer of de-ionized water in three horizontal rectangular silicon multi-microchannels heat sinks. These three heat sinks had channel width of 0.25 mm (D_h = 0.299 mm), 1 mm (D_h = 0.531 mm) and 2.2 mm (D_h = 0.64 mm) and fixed channel height of 0.4 mm. The heat transfer results of water exhibited nearly similar behaviour and conclusion to FC-77 where the effect of mass flux and channel width was insignificant in the two-phase region. Also, the pressure drop increased with decreasing channel width. It is difficult to draw clear conclusions on the aspect ratio effect from the work described in [5-8] as both the aspect ratio and the hydraulic diameter were varied. In addition, the experiments were not conducted with test section of the same or similar surface roughness.

Choi et al. [9-10] investigated experimentally the effect of channel aspect ratio on adiabatic two-phase flow of water and nitrogen gas in a horizontal rectangular glass microchannel. Four channels with different aspect ratio of 1.09, 1.5, 2.1 and 5.9 were tested. The hydraulic diameter was 0.49, 0.49, 0.322 and 0.143 mm. The range of liquid and gas superficial velocity was 0.06–1 m/s and 0.06–71 m/s respectively. They reported four flow regimes with the increase of gas superficial velocity, namely: bubbly, slug bubble, elongated bubble and liquid ring flows. They mentioned that the channel aspect ratio had a significant effect on the flow pattern characteristics. For example, when the channel aspect ratio increased (shallow channels), the liquid film around the elongated bubble gets thinner especially at the bottom and top walls of the channels and the liquid portion collected at the channel corners decreased. The pressure drop results indicated that flow patterns have a significant effect on the trend of pressure drop versus gas superficial velocity. The pressure drop increased linearly with increasing gas superficial velocity in bubbly, slug and elongated bubble flows. In the transition regime from elongated bubble to liquid ring flow, the pressure drop decreased linearly with increasing gas superficial velocity. When liquid ring flow was established, the pressure drop increased again linearly with increasing superficial gas velocity.

Soupremanien et al. [11] studied the effect of channel aspect ratio on the flow boiling heat transfer of Forane-365HX in a horizontal single rectangular minichannel. The bottom surface of the channel was made of brass with average roughness value of 2.5 μm, while the side walls were formed in stainless steel foil. They tested two test sections, width 2.3 mm and 5.6 mm and depth 1 mm and 0.8 mm giving a hydraulic diameter of 1.4 mm and aspect ratio of 2.3 and 7. In their study, the heat flux ranged from 2.3 to 160 kW/m^2 and the mass flux range was 200–400 kg/m^{2}s. The heat transfer results demonstrated that for the two investigated aspect ratios, the mass flux effect was insignificant. They stated that the two-phase pressure drop was lower in the channel with the larger aspect ratio due to the higher channel cross-sectional area. Additionally, the heat transfer coefficient in the channel with large aspect ratio was higher at low heat flux conditions, while it was lower at high heat fluxes due to dryout.

Fu et al. [12] studied the effect of channel aspect ratio on the flow boiling heat transfer of HFE-7100 in horizontal copper multi-microchannels with diverging cross section. They examined six test sections with a hydraulic diameter of 1.12 mm and average aspect ratio ranging from 0.16 to 1.2 at mass flux range of 39–180 kg/m^{2}s. They reported that channels with diverging cross section exhibited higher heat transfer rate and critical heat flux than channels with uniform cross section, especially at the lowest mass flux (G = 39 kg/m^{2}s). Additionally, they reported significant effect of aspect ratio on the boiling curve with channels of aspect ratio 0.99 showing the best performance due to the large liquid film thickness at the channel corners. However, inspecting the boiling curve in their paper, the effect of aspect ratio did not show a clear trend. Finally, they reported that a maximum base heat flux value of 1140 kW/m^2 was reached during their experiments.

Markal et al. [13] carried out an experimental investigation of flow boiling heat transfer of de-ionized water in horizontal rectangular multi-microchannels. Six heat sinks made of silicon with 29 microchannels were manufactured with channel aspect ratios of 0.37, 0.82, 1.22, 2.71, 3.54 and 5 and fixed hydraulic diameter of 0.1 mm. The experimental operating conditions were set at 50 °C inlet temperature, wall heat flux of 71–131 kW/m^2 and mass flux ranging from 151 to 324 kg/m^{2}s. Their boiling curve results demonstrated that boiling started at high wall superheat values, i.e. 30 K, in the channels with small aspect ratio of 0.37, 0.82 and 1.22. On the contrary, for the large channels with aspect ratio of 2.71, 3.54 and 5, boiling started at lower wall superheat, i.e. around 6 K. In other words, channels of nearly square cross section and deep channels perform worse than the shallow channels. They attributed this heat transfer behaviour to the periodic nature of the flow patterns that was observed in all channels. They reported that the flow patterns were fluctuating between rewetting, evaporation and slug-annular/annular flow and partial dryout. In the channels with high aspect ratios, the period of dryout was shorter compared to channels with smaller aspect ratio. They mentioned that, there was no regular relationship between the total pressure drop and the channel aspect ratio due to the complex flow boiling phenomenon.

Özdemir et al. [14] performed an experimental study of flow boiling heat transfer of water in a copper horizontal single microchannel at G = 200–800 kg/m^{2}s. They tested three test sections having the same hydraulic diameter (D_h = 0.56 mm) and aspect ratio of 0.5, 2.56 and 4.94. These channels had average surface roughness of 0.496, 0.139 and 0.102 μm. They reported four flow patterns namely; bubbly, slug, churn and annular flow that can occur periodically. The effect of aspect ratio on the flow patterns was found to be small except for bubbly flow. The bubbles were small in size and dispersed in the channel with larger aspect ratio and the bubbles became more elongated when the channel aspect ratio decreased due to the confinement effect. The heat transfer results indicated that, at heat flux up to 480–500 kW/m^2, the heat transfer coefficient increased with decreasing channel aspect ratio, while the effect of aspect ratio was insignificant at higher heat fluxes.

It can be concluded from the above experimental studies that the effect of channel aspect ratio on the flow patterns, two-phase pressure drop and heat transfer coefficient is still unclear and more investigation is required. In some studies, the effect of aspect ratio was investigated while the hydraulic diameter and average surface roughness were not fixed. Additionally, some researchers studied the effect of aspect ratio at operating conditions near boiling incipience, i.e. at very low vapour qualities and heat fluxes. Accordingly, it is difficult to get a general conclusion about the effect of channel aspect ratio. Therefore, the present study examined the effect of channel aspect ratio on flow patterns, pressure drop and heat transfer characteristics while keeping the average surface roughness and hydraulic diameter fixed. Three heat sinks made of oxygen-free copper with hydraulic diameter of 0.46 mm and different channel aspect ratios of 0.5, 1 and 2 were examined. The average surface roughness of all channels was measured and was

Table 1
Thermophysical properties of HFE-7100 at 1 bar obtained from EES software.

i_{lg} [J/kg]	ρ_l [kg/m^3]	ρ_g [kg/m^3]	k_l [W/mK]	C_p [J/kgK]	σ [N/m]
111,661	1373	9.575	0.06206	1157	0.0136

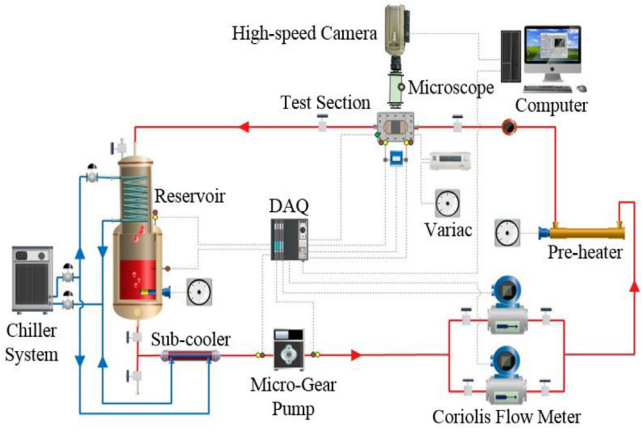

Fig. 1. Schematic diagram of the experimental facility [28].

approximately 0.3 μm. All the experiments were carried out using fluid HFE-7100 at system pressure near 1 bar, low inlet sub-cooling of 5 K, mass flux ranging from 50 to 250 kg/m^{2}s and wall heat flux from 9.6 to 191.6 kW/m^2. The thermophysical properties of the tested fluid at atmospheric pressure are presented in Table 1.

2. Experimental system

2.1. Flow loop

The experimental facility, as shown in Fig. 1 and 2, was a closed flow loop that consisted of liquid reservoir (9 L volume), sub-cooler (heat exchanger), micro-gear pump with digital driver, two Coriolis flow meters (for low and high mass flow rates), pre-heater, data logger, test section (evaporator) and condenser. The reservoir included an immersion heater and the condenser cooling coil was mounted on the topside of this reservoir. The immersion heater and the condenser were also used to adjust the system pressure and to degas the liquid before the experiments by vigorous boiling. The sub-cooler was installed before the pump to avoid fluid cavitation. The micro-gear pump supplied flow rate up to 2304 mL/min. This flow rate was measured using the two Coriolis flow meters with accuracy of ±0.1%. A stainless steel pre-heater with heating power of 1500 W was installed before the test section to control the fluid inlet temperature, i.e. the fluid inlet sub-cooling. The supplied power to the reservoir, pre-heater and the test section was controlled by three Variac transformers. The input power to the test section was measured using a power metre (Hameg HM8115–2) with accuracy of ±0.4%. A chiller system with 2.9 kW cooling capacity was connected to the rig to reject the heat from the reservoir and the sub-cooler. All the measuring sensors, such as thermocouples, inlet/outlet pressure transducers, differential pressure transducer and flow meters were connected to the National Instruments Data Acquisition System-DAQ with a frequency of 1 kHz. A Phantom high-speed camera with 1000 fps at 512 × 512 pixel coupled with a Huvitz HSZ-645TR microscope and LED lighting system were used to capture the two-phase flow patterns.

2.2. Test section

The test section consisted of the bottom plate, the housing, the cover plate and the heat sink block as illustrated in Fig. 3(a). A Polytetrafluoroethylene block was used to fabricate both the housing and the bottom plate to ensure a good insulation. Twelve holes, with a diameter of 0.6 mm, were drilled into this housing to pass the thermocouple wires. In order to capture the flow patterns during the experiments, a transparent polycarbonate cover plate was manufactured. Both the inlet and outlet plena, with semi-circular shape, were formed in the top cover. The heat sink block was made of oxygen-free copper with 26 mm width, 94.5 mm height and 51 mm length as shown in Fig. 3(b). Four cartridge heaters of 700 W total heating power were vertically inserted into the heat sink block from the bottom side. Four tapping holes were drilled into the cover plate, see Fig. 3(c) in order to insert the measuring sensors, i.e. inlet/outlet fluid thermocouples, inlet/outlet pressure transducers and one differential pressure transducer. This plate was placed on the topside of the housing, and an O-ring was inserted between this plate and the heat sink to prevent any fluid leakage. Twelve K-type thermocouples were inserted into the

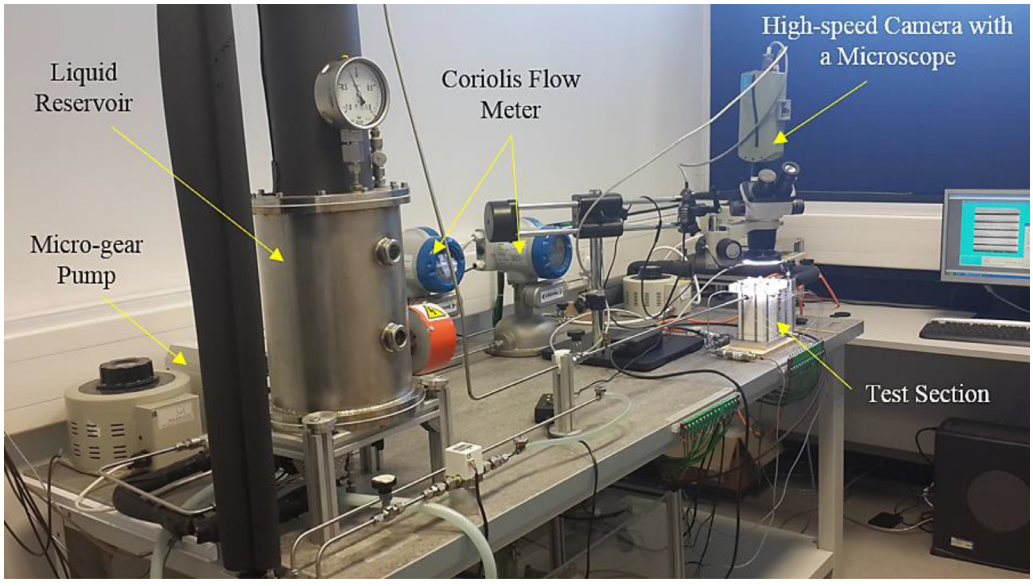

Fig. 2. Photograph of the experimental facility.

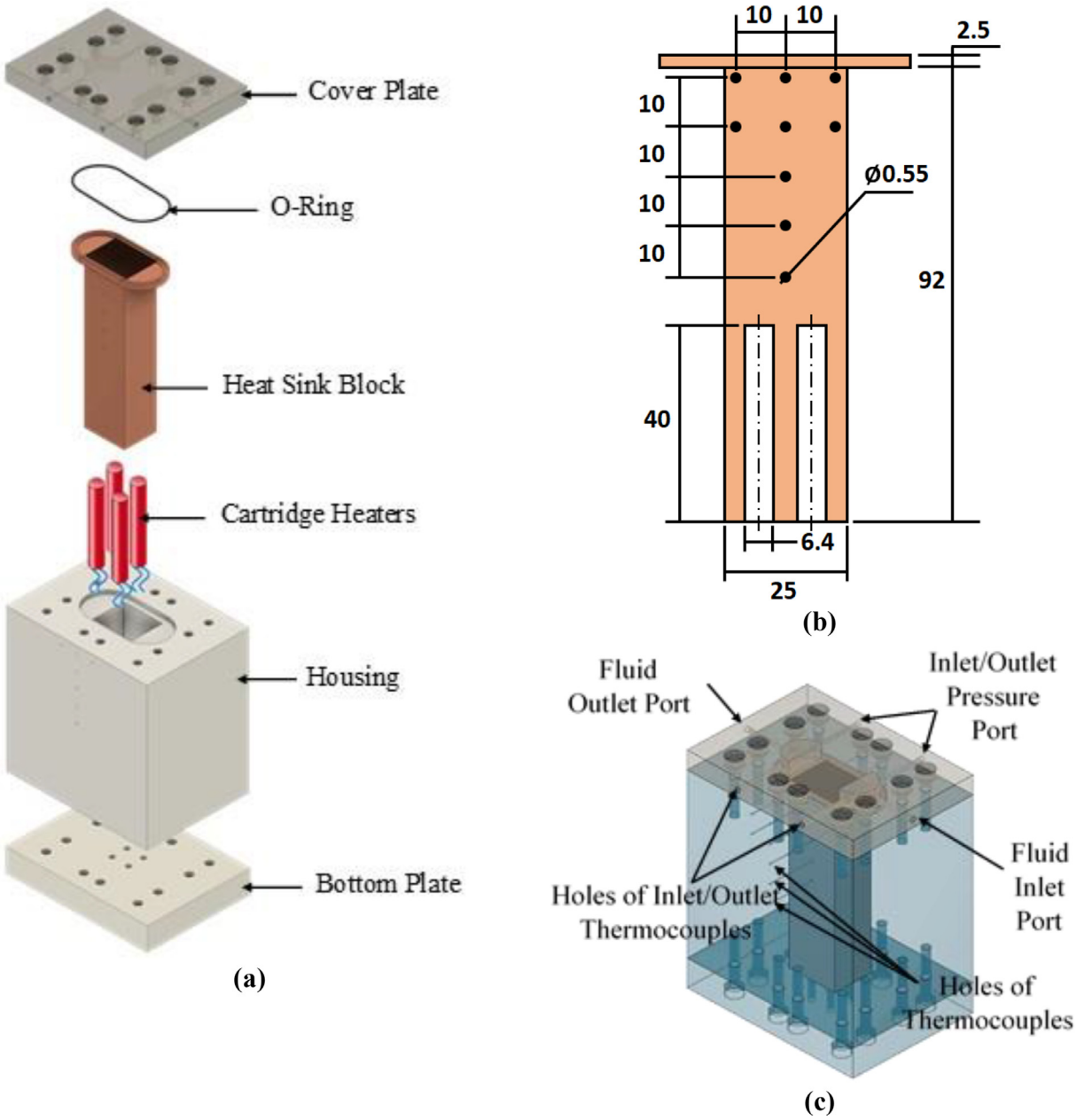

Fig. 3. Test section details (a) Exploded drawing and (b) Heat sink block, dimensions in mm [28] (c) Overall assembly.

heat sink block, see Fig. 3(c), to assess the temperature distribution along the channels, in the transverse and vertical direction. Three of these thermocouples were located in the axial direction parallel to the flow at the opposite side of the block. These thermocouples help to measure the base heat flux and to help confirm that there was no heat flow in the horizontal and transverse directions, i.e. 1D heat conduction in the vertical direction.

2.3. Microchannels heat sink

In this study, three heat sinks with different channel aspect ratios were fabricated using a high-precision milling machine (Kern HSPC-2216). Rectangular multi-microchannels were milled on the top surface of the heat sink block. These horizontal microchannels have the same channel hydraulic diameter of 0.46 mm and same channel length of 25 mm, but different aspect ratios, i.e. 0.5, 1 and 2. The number of channels was 40, 36 and 25 respectively. The base area of the heat sink was calculated from the width and length which were 20 and 25 mm, respectively. This base area of 500 mm^2 was chosen based on the chipset die size. It is known that the value of die size differs from chipset to another according to the chipset performance. For example, the die size of Intel Sandy Bridge 4C processor is 216 mm^2 and is 503 mm^2 for Intel Xeon E7440 (source: www.intel.com). In the present study, both the microchannels and the inlet and outlet plena with semi-circular shape were designed as one part. This was adopted to (i) design microchannels heat sink that is acceptable for commercial applications, i.e. this ensures an integrated assembly and a flat surface bottom, which can easily be attached to any chipset, and (ii) prevent any leakage that could happen during the experiments by inserting O-ring around the heat sink. The bottom thickness of the inlet and outlet plena was very thin, i.e. just 2 mm, to ensure minimum heat transfer in these parts. This minimum size of 2 mm was necessary for strength, i.e. avoid possible break at this point.

Table 2
Geometric dimensions of the test sections.

Test section	H_{ch} [mm]	W_{ch} [mm]	W_{fin} [mm]	N [-]	D_h [mm]	β [-]	$W_b \times L_b$ [mm]	R_a [μm]
1	0.7	0.35	0.15	40	0.46	0.5	20 × 25	0.271
2	0.46	0.46	0.1	36	0.46	1	20 × 25	0.286
3	0.35	0.7	0.1	25	0.46	2	20 × 25	0.304

It is worth mentioning that the machining conditions, i.e. cutting feed rate and rotation speed, affect the channel surface microstructures and thus the surface roughness. Accordingly, the machining conditions were kept the same during the fabrication of all heat sinks. The spindle of the machine was set at a cutting feed rate and rotation speed of 550 mm/min and 20,000 rpm, respectively. Therefore, the average surface roughness of all microchannels was approximately the same value. A surface profiler instrument, Zygo NewView 5000, was used to measure the channel bottom roughness at different locations then the average value was taken. It was found that the average surface roughness of the three heat sinks was 0.271, 0.286 and 0.304 μm. Fig. 4 shows the surface characteristics, for the test section with aspect ratio of 0.5, over a sample test area of 0.132 × 0.176 mm. This figure depicts the intensity map, the surface profile and the surface map (2D and 3D). It can be seen that the surface average roughness is 0.27 μm, while the minimum valley depth and the maximum peak height are 1.57 and 1.86 μm, respectively. It also shows the maximum peak to valley height, which is 3.43 μm over this area. The dimensions and average roughness for each test section are presented in Table. 2. All the channel dimensions were measured using an optical coordinate measuring machine (TESA-VISIO 200GL) with accuracy of ±2 μm.

3. Data reduction

During the single-phase experiments, the experimental Fanning friction factor f_{exp} and the average Nusselt number $\overline{Nu}$ were calculated as follow:

$$f_{exp} = \frac{\Delta P_{ch} D_h}{2 L_{ch} \nu_l G_{ch}^2} \tag{1}$$

$$\overline{Nu} = \frac{\bar{h} D_h}{k_l} \tag{2}$$

where ΔP_{ch}, D_h, L_{ch}, ν_l, G_{ch}, $\bar{h}$ and k_l are the channel pressure drop, the channel hydraulic diameter, the channel length, the liquid specific volume, the channel mass flux, the average heat transfer coefficient and the liquid thermal conductivity, respectively. The channel pressure drop was calculated from the total measured pressure drop ΔP_{meas} and the pressure drop components as shown in Eq. (3).

$$\Delta P_{ch} = \Delta P_{meas} - \left(\Delta P_{ip} + \Delta P_{sc} + \Delta P_{se} + \Delta P_{op}\right) \tag{3}$$

The pressure drop components ΔP_{ip}, ΔP_{sc}, ΔP_{se} and ΔP_{op} are the pressure drop in the inlet plenum due to the change in flow direction by 90°, the sudden contraction pressure drop at the channel inlet, the sudden expansion pressure drop at the channel outlet and the pressure drop in the outlet plenum due to the change in flow direction by 90°, respectively. These components can be calculated using a procedure described by Remsburg [15] as follows:

$$\Delta P_{ip} = K_{90} \frac{1}{2} G_p^2 \nu_l \tag{4}$$

$$\Delta P_{op} = K_{90} \frac{1}{2} G_p^2 \nu_l \tag{5}$$

$$\Delta P_{sc} = \frac{1}{2} G_{ch}^2 \nu_l \left[1 - \alpha^2 + 0.5(1-\alpha)\right] \tag{6}$$

$$\Delta P_{se} = \frac{1}{2} G_{ch}^2 \nu_l \left[\frac{1}{\alpha^2} - 1 + (1-\alpha)^2\right] \tag{7}$$

where K_{90} and α are the loss coefficient of the 90^0 turns and the area ratio ($\alpha = \frac{A_{min}}{A_{max}}$), respectively. The uniform wall temperature method (UWT) was adopted here to calculate the average heat transfer coefficient and thus the average Nusselt number. Eq. (8) was used to calculate the heat transfer coefficient.

$$\bar{h} = \frac{q''_b W_b L_{ch}}{A_{ht} \Delta T_{LM}} \tag{8}$$

where q''_b, W_b, A_{ht} and ΔT_{LM} are the base heat flux, the base width, the total heat transfer area and the log mean temperature difference, respectively. The log mean temperature difference can be calculated as follows:

$$\Delta T_{LM} = \frac{T_{fo} - T_{fi}}{\ln\left(\frac{T_{wi} - T_{fi}}{T_{wi} - T_{fo}}\right)} \tag{9}$$

The vertical wall temperature gradient $\frac{dT}{dy}$ was used to estimate the base heat flux q''_b as follows:

$$q''_b = k_{cu} \left.\frac{dT}{dy}\right|_{y=0} \tag{10}$$

where k_{cu} is the copper thermal conductivity. Eq. (11) was used to calculate the total heat transfer area A_{ht} by assuming uniform heat flux in the axial and transverse direction and three-sides heated (adiabatic cover plate).

$$A_{ht} = (2H_{ch} + W_{ch}) L_{ch} N \tag{11}$$

where H_{ch}, W_{ch} and N are the channel height, width and the number of channels, respectively. During the two-phase experiments, the heat transfer coefficient and the vapour quality were calculated locally, i.e. at three locations along the channel, see Eq. (12) and (13).

$$h_{(z)} = \frac{q''_b (W_{ch} + W_{fin})}{(T_{wi(z)} - T_{f(z)})(W_{ch} + 2\eta H_{ch})} \tag{12}$$

$$x_{(z)} = \frac{i_{(z)} - i_{l(z)}}{i_{\mathrm{lg}\,(z)}} \tag{13}$$

where W_{fin}, $T_{wi(z)}$, $T_{f(z)}$, η, $i_{(z)}$, $i_{l(z)}$ and $i_{\mathrm{lg}(z)}$ are the fin width, the local internal surface temperature, the local fluid temperature, the fin efficiency, the local specific enthalpy, the local liquid specific enthalpy and the local latent heat of vaporization, respectively. The fin efficiency η can be calculated using Eq. (14) and (15).

$$\eta = \frac{\tanh(mH_{ch})}{mH_{ch}} \tag{14}$$

$$m = \sqrt{\frac{2h_{(z)}}{k_{cu} W_{fin}}} \tag{15}$$

Eq. (16) was used to calculate the local internal surface temperature.

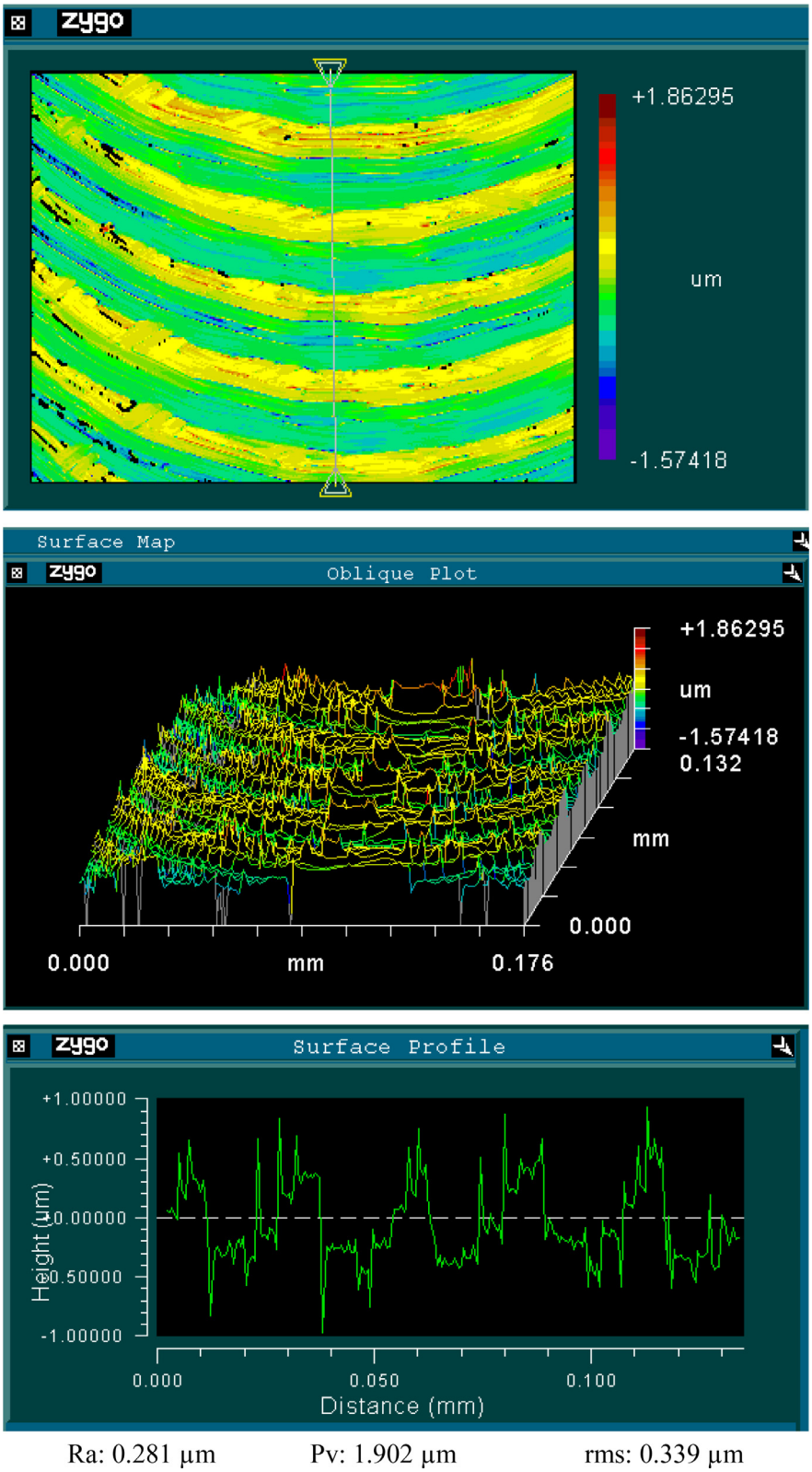

Fig. 4. Surface characteristics of the channel bottom for aspect ratio 0.5 using Zygo NewView 5000.

$$T_{wi(z)} = T_{th(z)} - \frac{q''_b b}{k_{cu}} \tag{16}$$

where $T_{th(z)}$ is the local thermocouple temperature, while b is the vertical distance between the thermocouple and the channel bottom. The local fluid temperature $T_{f(z)}$ can be calculated using Eq. (17).

$$T_{f(z)} = T_{fi} + \frac{q''_b W_b z}{\dot{m} c p_l} \tag{17}$$

The local fluid temperature $T_{f(z)}$ was used during liquid single-phase region. This temperature was replaced by the local satura-

tion temperature during two-phase flow region. The local saturation temperature was found from the corresponding local pressure $P_{sat(z)}$ by assuming a linear pressure drop along the channel, see Eq. (18).

$$P_{sat(z)} = P_{sat(z,sub)} - \left(\frac{z - L_{sub}}{L_{ch} - L_{sub}}\right)\Delta P_{tp} \tag{18}$$

where $P_{sat(z,\ sub)}$, z, L_{sub}, L_{ch} and ΔP_{tp} are the local saturation pressure at the subcooled region, the axial distance, the subcooled length, the channel length and the two-phase pressure drop, respectively. The local saturation pressure at the subcooled region and the subcooled length (length of single-phase region) were calculated as follows:

$$P_{sat(z,sub)} = P_i - \frac{2fG_{ch}^2 L_{sub}}{\rho_l D_h} \tag{19}$$

$$L_{sub} = \frac{\dot{m}cp_l\left(T_{sat(z,sub)} - T_{fi}\right)}{q''_b W_b} \tag{20}$$

where P_i and f are the inlet pressure and the Fanning friction factor, respectively. The Fanning friction factor was calculated using Eqs. (21-23) for developing laminar flow as proposed by Shah and London [16].

$$f_{app} = \frac{3.44}{Re\sqrt{L^*}} + \frac{f_{FD}Re + \frac{K_\infty}{4L^*} - 3.44/\sqrt{L^*}}{Re\left(1 + C(L^*)^{-2}\right)} \tag{21}$$

$$L^* = L_{sub}/ReD_h \tag{22}$$

$$f_{FD}Re = 24(1 - 1.355\beta + 1.946\beta^2 - 1.7012\beta^3 + 0.9564\beta^4 - 0.2537\beta^5) \tag{23}$$

where L^*, β, C and K_∞ are the dimensionless length, the channel aspect ratio, the dimensionless correction factor and the dimensionless incremental pressure drop number, respectively. Both C and K_∞ were found from Shah and London [16]. An iteration process was conducted between Eq. (19) and (20) to find the local saturation temperature at the end of the subcooled region $T_{sat(z,\ sub)}$, corresponding to the local saturation pressure at the subcooled region $P_{sat(z,\ sub)}$, and then determine the subcooled length L_{sub}. The two-phase pressure drop ΔP_{tp} in Eq. (18) was calculated by subtracting the channel pressure drop from the single-phase pressure drop. The local specific enthalpy $i_{(z)}$ in Eq. (13) was calculated as follows:

$$i_{(z)} = i_i + \frac{q''_b W_b z}{\dot{m}} \tag{24}$$

The average heat transfer coefficient along the channel is given in Eq. (25).

$$\bar{h} = \frac{1}{L_{ch}} \int_0^{L_{ch}} h_{(z)} dz \tag{25}$$

Table 3 presents the experimental uncertainties for all variables. The uncertainty values of the measured variables, i.e. thermocouples and inlet/outlet pressure transducers, were calculated from the calibration procedure. The uncertainties of the differential pressure transducer and Coriolis flow meters were found from the manufacturer specification datasheets. The uncertainties of all derived variables were calculated using the procedure proposed by Coleman and Steele [17].

4. Experimental procedure

In this study, single and two-phase experiments were conducted at different operating conditions. Before starting any experiment, flashing and degassing processes were carried out to ensure that there is no trapped gas in the test section and the test loop. The micro-gear pump run at high mass flow rate to push any trapped gases to the liquid reservoir. Since the fluid HFE-7100 contains 53% of air by volume under ambient condition [18], a degassing process was carried out, see Al-Zaidi et al. [19] for more details about this process. It is worth mentioning that the rig was charged with pure HFE-7100 (the fluid was not exposed to the atmosphere before charging) under vacuum, i.e. minimal traces of dissolved gases. Single-phase experiments were performed at adiabatic and diabatic conditions to valid the experimental rig using the single-phase Fanning friction factor and the average Nusselt number. Flow boiling experiments were conducted at five mass fluxes and exit vapour quality up to 0.99 as presented in Table 4. Steady state conditions were assumed when the variation in the measuring signals of temperature, pressure and mass flow rate was less than 5%. Data were then collected for two minutes at a frequency of 1 kHz via LabView software and saved. The average value was then used in all calculations adopted in the data reduction. The EES software was used to obtain all the thermophysical properties of the tested fluid and to develop the calculations program. Flow visualization was recorded for each run at the heat sink centre and at three different locations; near the channel inlet, near the middle and near the channel outlet.

Table 3
Experimental uncertainties.

Parameter	Uncertainty
Temperature T-type	±0.024K
Temperature K-type	±0.038–0.12K
Inlet pressure transducer	±0.46kPa
Outlet pressure transducer	±0.37kPa
Differential pressure	±0.08%
Coriolis mass flow rate	±0.1%
Fanning friction factor	±1.46–2.99%
Average Nusselt number	±1.4 – 11.9%
Local vapour quality	±0.35–15.3%
Local heat transfer coefficient	±0.72–13.48%
Mass flux	±0.32–0.64%
Heat flux	±0.12–6.88%

Table 4
Experimental operating conditions.

System pressure [bar]	1
Saturation temperature [°C]	59.63
Inlet sub-cooling [K]	5
Mass flux [kg/m^{2}s]	50–250
Base heat flux [kW/m^2]	Up to 531.2
Exit vapour quality [-]	Up to 0.99

5. Results and discussions

5.1. Single-phase validation

The experimental system and measuring instruments were validated using single-phase experiments. Fig. 5 shows the experimental Fanning friction factor plotted versus Reynolds number for the channels with aspect ratio of 0.5 and compared with the correlation by Shah and London [16] for horizontal non-circular channels. This figure depicts that the experimental results were in a good agreement with Shah and London correlation for developing flow. Fig. 6 presents the experimentally determined average Nusselt number versus Reynolds number compared with three existing correlations such as Shah and London [16] for developing flow, Peng and Peterson [20] and Mirmanto [21]. It shows that the Nusselt number increased with Reynolds number, and there was a reasonable agreement with the correlations by Peng and Peterson [20] and Mirmanto [21] giving a mean absolute difference of 11% and 14%, respectively.

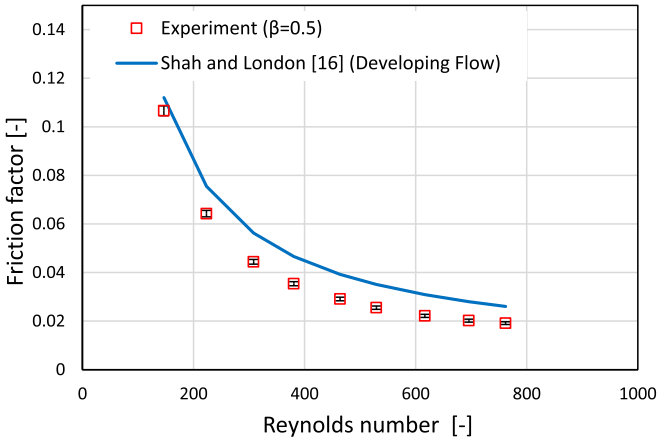

Fig. 5. Experimental Fanning friction factor versus Reynolds number for aspect ratio of 0.5.

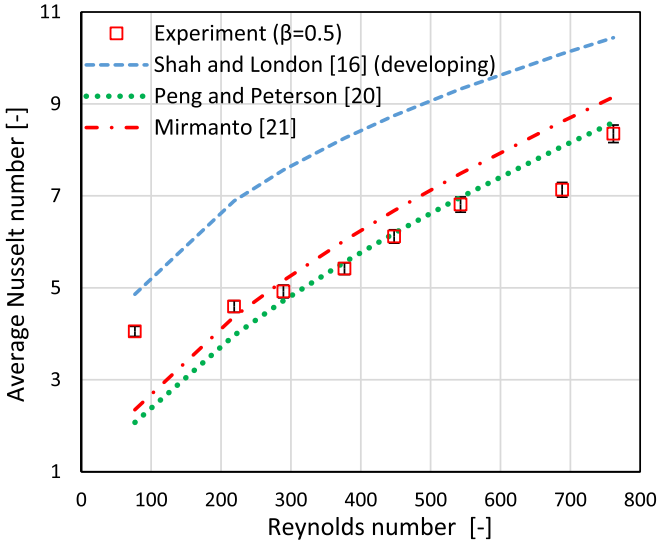

Fig. 6. Average Nusselt number versus Reynolds number for aspect ratio of 0.5.

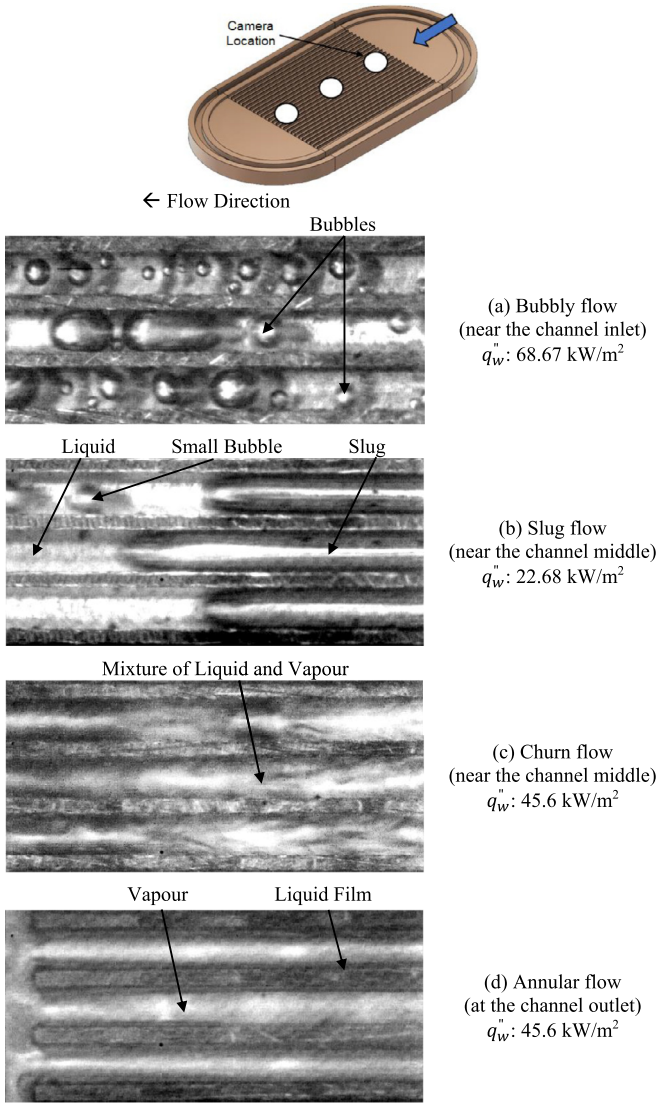

Fig. 7. Experimental flow patterns at mass flux of 100 kg/m^{2}s for the channel aspect ratio of 0.5.

5.2. Flow boiling patterns

The experimental flow patterns were observed at different locations along the centre of the heat sink. The size of each photograph taken by the present camera was 4 × 4 mm. Four flow patterns were observed in the three examined test sections, namely: bubbly, slug, churn and annular flow. Fig. 7 illustrates the features of these flow patterns for mass flux 100 kg/m^{2}s and channel aspect ratio of 0.5. Fig. 7(a) shows that bubbly flow with bubble size smaller than the channel width was observed near the channel inlet at wall heat flux of 68.67 kW/m^2. Bubbly flow was observed near the channel inlet for the entire heat flux range studied. Some of these bubbles were observed to nucleate at the channel corners, while some of them became confined. Slug flow was observed near the channel middle at wall heat flux of 22.68 kW/m^2 and higher as a long cylindrical vapour bubble followed by bubbles as illustrated in Fig. 7(b). Churn flow was captured near the channel middle at wall heat flux of 45.6 kW/m^2 and higher which was characterized by non-uniform vapour-liquid interphase and shape, as depicted in Fig. 7(c). Annular flow occurred at the channel outlet, when wall heat flux was 45.6 kW/m^2 and higher as a vapour core surrounded by liquid film, see Fig. 7(d). In addition to the previous regimes, Fig. 8 depicts an interesting feature, which was observed at high heat fluxes, i.e. the presence of bubble nucleation in the liquid film of annular flow at the channel corners, see also Karayiannis and Mahmoud [1]. This photograph was taken near the channel middle at wall heat flux of 51 kW/m^2 and mass flux of 200 kg/m^{2}s for the smaller channel aspect ratio. This was visualised for all test sections and could be due to the high wall superheat activating more nucleation sites at high heat fluxes. Magnini and Matar [22] conducted a numerical study to investigate the effect of channel aspect ratio ($\beta = 1$–8) on flow boiling characteristics of a single bubble under uniform heat flux boundary condition. They seeded a small bubble at the centre of the channel cross section and allowed for evaporation at the liquid-vapour interface without considering any nucleation. Their results indicated that the degree of superheat was much higher at the channel corners for all examined aspect ratios. Additionally, in the square channel, the liquid film was too thin at all walls except at the channel corners. In rectangular channels, when the aspect ratio increased (shallow channel), the liquid film was too thin at the top and bottom walls and too thick at the side walls, e.g. it was about 80% of the perimeter for $\beta > 4$. The high wall superheat and thick liquid film (either at the corners or side walls) could promote nucleation in the liquid film, which agrees with the current study, see Fig. 8.

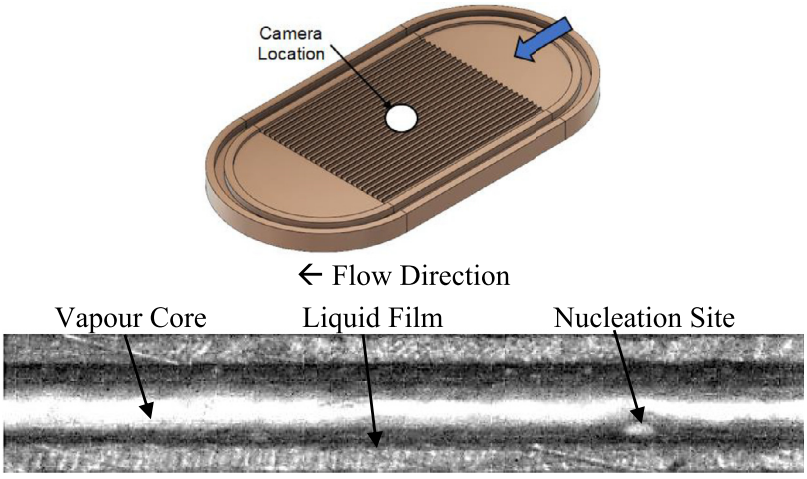

Fig. 8. Nucleation site in the liquid film of annular flow at wall heat flux of 51 kW/m^2 and mass flux of 200 kg/m^{2}s for aspect ratio of 0.5 (near the channel middle).

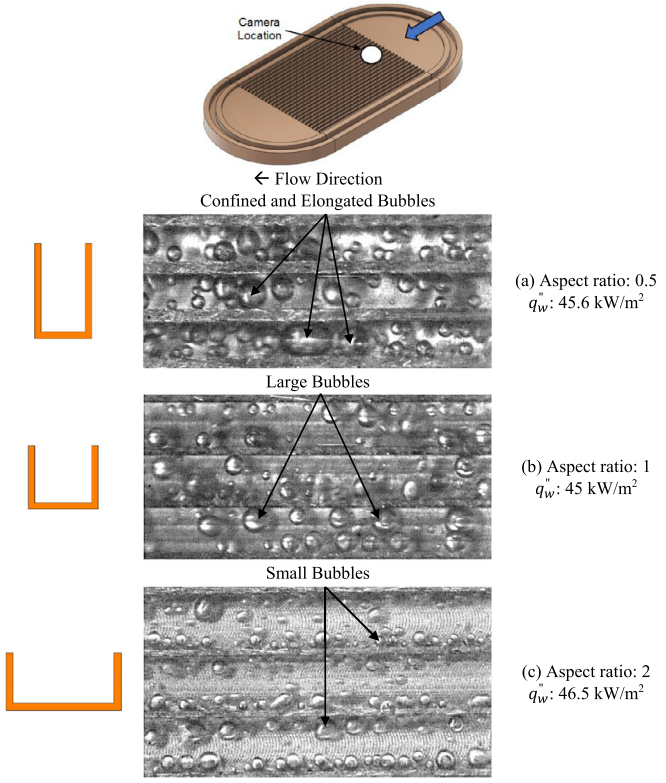

Fig. 9. Bubbly flow at wall heat flux near 45 kW/m^2 and mass flux of 100 kg/m^{2}s for different channel aspect ratios (near the channel inlet).

Although bubbly, slug, churn and annular flow were visualized for all channel aspect ratios, slight differences in their features were found. Fig. 9 shows the features of bubbly flow observed near the channel inlet at wall heat flux near 45 kW/m^2, mass flux of 100 kg/m^{2}s and different aspect ratios. Fig. 9(a) demonstrates that, for the channel with aspect ratio of 0.5, the size of the bubbles was smaller than the channel width. However, larger confined bubbles were also present. For the channel with aspect ratio of 1, the bubble size was still smaller than the channel width, see Fig. 9(b), and the bubbles size was smaller than that observed in the channels with aspect ratio of 0.5. Some of the bubbles became larger due to bubble coalesence and their size approached the channel width. For the channel of larger aspect ratio, i.e. aspect ratio of 2, the bubble size was much smaller than the channel width and smaller than those seen in the other apsect ratios, see Fig. 9(c). These differences in the bubble size are likely due to the strong effect of confinement induced by the channel walls when the channel width decreases and possible heat transfer from all three heated walls. It can be concluded from Fig. 9 that the bubble size increases as the channel aspect ratio decreases (reduction in the channel width). Another reason for the difference in bubble size observed in the three test sections could be the effect of flow reversal. In the present study, flow reversal and pressure drop fluctuation were found to increase with decreasing channel aspect ratio for the mass flux ranged studied. With flow reversal, the mass flux may vary amongst the channels which has a significant effect on bubble size. Moreover, the bubble size may become large during the stagnation period due to more evaporation rate from surrounding and coalescence rate, see Section 5.3.

Fig. 10 depicts the effect of aspect ratio on the features of slug flow observed near the channel middle at wall heat flux near 23 kW/m^2 and mass flux of 50 kg/m^{2}s. Vapour slugs, which filled the channel cross-sectional area were seen in all test sections. These slugs were followed by small and large bubbles, as shown in this figure. The figure illustrates that the size of these bubbles and the slug ends differed from channel aspect ratio to another. When the channel aspect ratio decreased, the slug ends had more round shape due to the fact that these slugs were squeezed by the channel sidewalls. Moreover, the bubbles that followed the slugs became larger (more confined) with decreasing channel aspect ratio due to the confinement effect.

Fig. 11 illustrates the effect of aspect ratio on the features of annular flow at wall heat flux near 79 kW/m^2 and mass flux of 250 kg/m^{2}s. This photograph was taken at the channel outlet. It can be seen that, there was no clear effect of aspect ratio on annular flow. It is worth mentioning that it was difficult to measure the distrubtion and thickness of the liquid film in this regime, even with the high-speed, high-resolution camera used in this study.

It can be concluded from the above discussion that the three investigated aspect ratios do not show significant effects on the observed flow patterns. The effect of aspect ratio could be limited to the slug flow, see above. The effect of aspect ratio could affect the distribution and thickness of the liquid film, which however could not be captured in the present study using the high speed camera, which views from the top side.

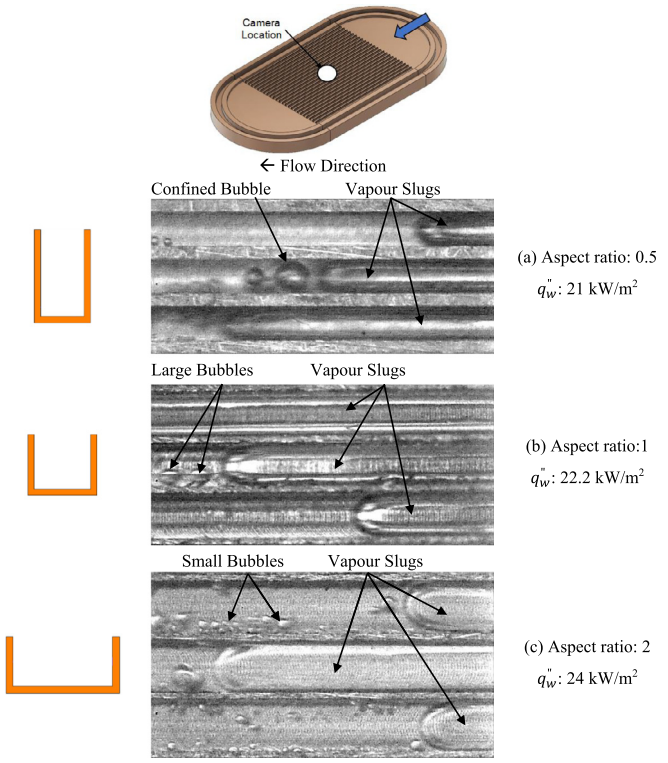

Fig. 10. Slug flow at wall heat flux near 23 kW/m^2 and mass flux of 50 kg/m^{2}s for different channel aspect ratios (near the channel middle).

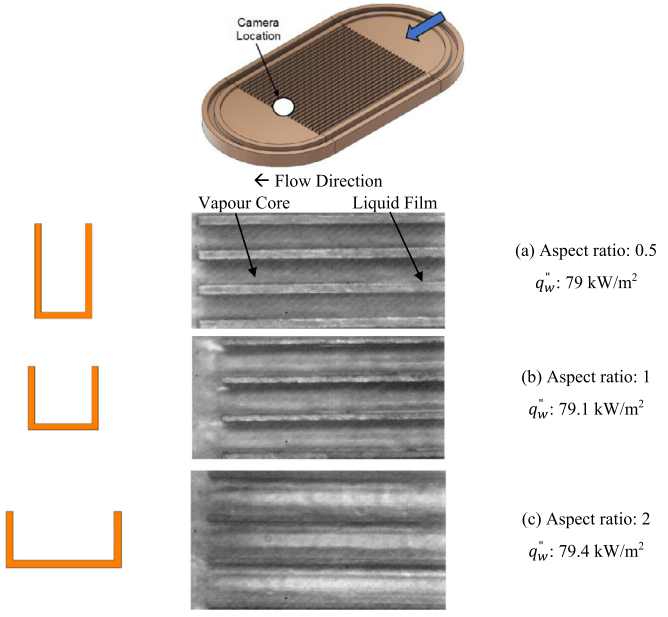

Fig. 11. Annular flow at wall heat flux near 79 kW/m^2 and mass flux of 250 kg/m^{2}s for different channel aspect ratios (at the channel outlet).

5.3. Flow reversal and instability

Flow reversal and fluctuations in pressure, mass flux and temperature are very common in multi-microchannels configurations. Flow reversal is a periodic back flow due to a sudden increase in the flow resistance inside the microchannels. Kandlikar [23] attributed flow reversal to the occurrence of bubble nucleation near the channel inlet and the low flow resistance to back flow. In other words, the high evaporation rate leads to an increase in the evaporation momentum force, which when exceeds the shear and inertia forces results in flow reversal as mentioned by Kandlikar [24]. High pressure and mass flux fluctuations are other indicators of flow instability. Flow reversal was reported in some experimental studies, see Chen and Garimella [25], Yang et al. [26] and Fayyadh et al. [27]. In the present study, flow reversal occurred after boiling incipience for all examined heat and mass fluxes. This could be due to the bubble generation near the channel inlet and slug formation as captured by the camera, see Al-Zaidi et al. [28] for further discussion.

Fig. 12 depicts a sequence of pictures of flow reversal for channel aspect ratio of 2 at wall heat flux of 114.8 kW/m^2 and mass flux of 250 kg/m^{2}s. These pictures were taken at a location between the channel inlet and middle to detect the cycle of flow reversal. The flow reversal cycle was found to be forward, stagnation and backward motion. Moreover, the experimental flow patterns were fluctuating between bubbly, confined bubbles and slug flow. At an arbitrary starting time of 0 ms, small bubbles moved towards the channel outlet. These bubbles had size smaller than the channel width. After 21 ms, the captured bubbles stayed at their locations for about 1 ms. During this stagnation period, the bubbles size became larger due to heat transfer from the surrounding and coalescence with others. After that, back motion was visualized with continuous increase in bubble size until the bubbles became confined at 27 ms. After 37 ms, all the channels were filled with vapour slugs that moved towards the channel inlet. This period (backward motion) took about 21 ms. At time of 43 ms, the cycle of flow reversal was finished and small new bubbles occurred inside the channels that moved to the downstream direction.

Flow reversal is very common in multi-microchannels, regardless of channel geometry and operating conditions (heat and mass flux). Therefore it would be difficult to infer the effect of aspect ratio using the sequence of flow patterns discussed above in Fig. 12. In other words, this figure is presented to explain the mechanism and phenomenon of flow reversal but cannot be used to understand the effect of aspect ratio. The high speed camera and the pressure sensors should be synchronized in order to have a link between the pressure signals and flow patterns. In the present study, pressure and temperature measurements were conducted simultaneously but not synchronized. Accordingly, the pressure drop signal is used to quantify the effect of aspect ratio on flow instability, as depicted in Fig. 13 for $G = 150$ kg/m^{2}s at low and high wall heat fluxes. The figure shows that the pressure drop fluctuation increased when the channel aspect ratio decreased. For example, the amplitude of fluctuation increased from 0.16 to 1.15 kPa when the channel aspect ratio decreased from 2 to 0.5 at wall heat flux near 53 kW/m^2. This effect was also found at high wall heat flux, i.e. 70 kW/m^2, as shown in Fig. 13(b). As mentioned above, because the pressure drop measurements and the flow visualisation were not synchronised, it was difficult to link directly the higher amplitude of the pressure fluctuation in the channel of $\beta = 0.5$ to flow instabilities and flow reversal. Thus, based on the pressure drop signal, it can clearly be stated that the instabilities are higher in the small aspect ratio channels.

It can be concluded from the above discussion that pressure drop fluctuation increases as the aspect ratio decreases. However, it must be emphasised that the heat transfer results in this study were not significantly affected by this mild flow reversal. This can be confirmed by checking the measured signal of inlet/outlet pressure, inlet/outlet fluid temperature and wall temperatures along the channel for all heat sinks. The maximum percentage of fluctuation was found to be 2.37% for the inlet pressure, 1.11% for the outlet pressure, 0.85% for the inlet fluid temperature, 0.04% for the outlet fluid temperature and between 0.05% to 0.46% for the wall temperature, see Fig. 14, which shows the inlet pressure fluctuation for three heat sinks. Al-Zaidi et al. [28] also presented the

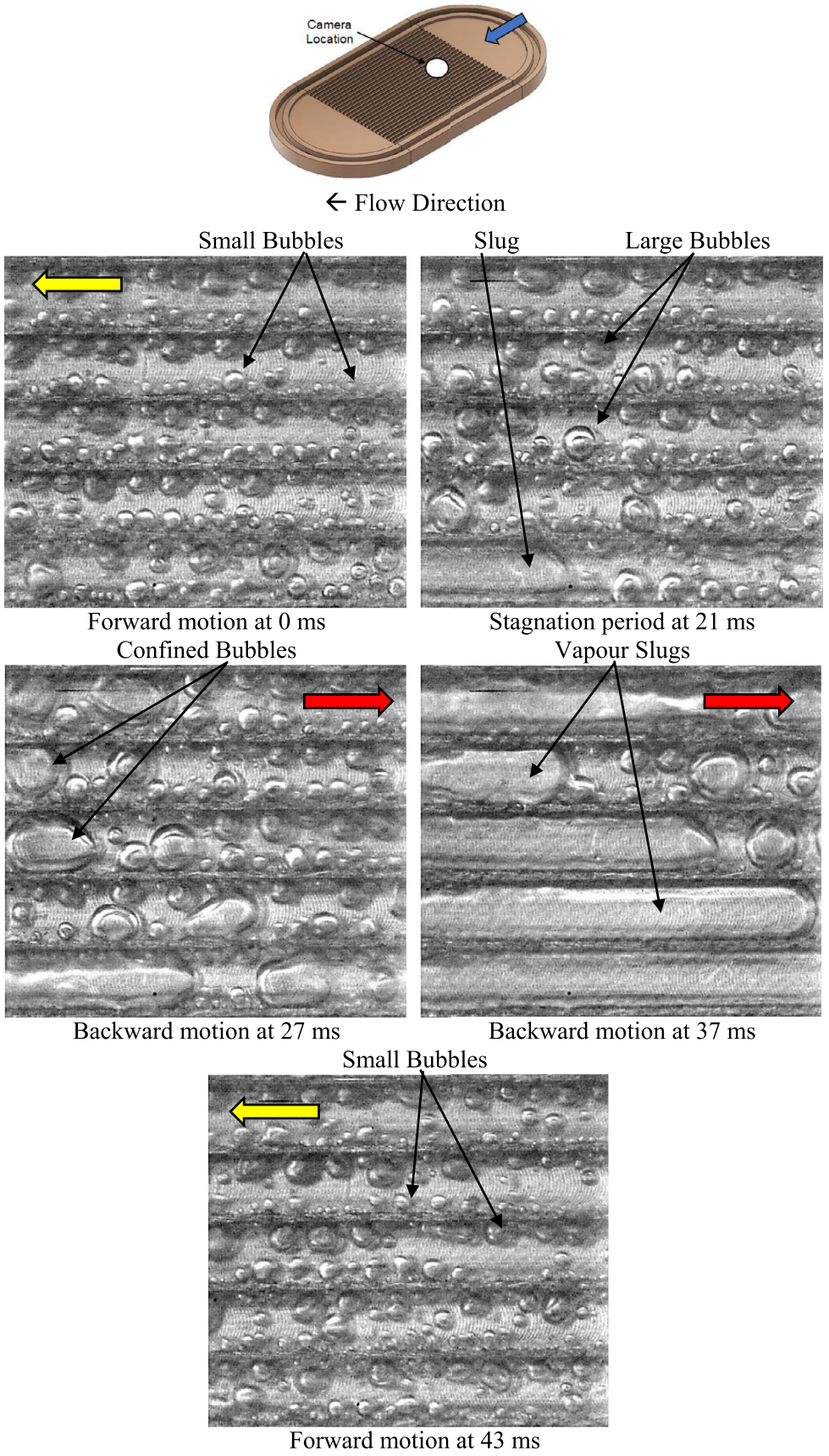

Fig. 12. Sequence of pictures of flow reversal for aspect ratio of 2 at wall heat flux of 114.8 kW/m^2 and mass flux of 250 kg/m^{2}s (between the channel inlet and middle). Yellow arrow indicates forward motion and red backward motion. (For interpretation of the references to colour in this figure legend, the reader is referred to the web version of this article.)

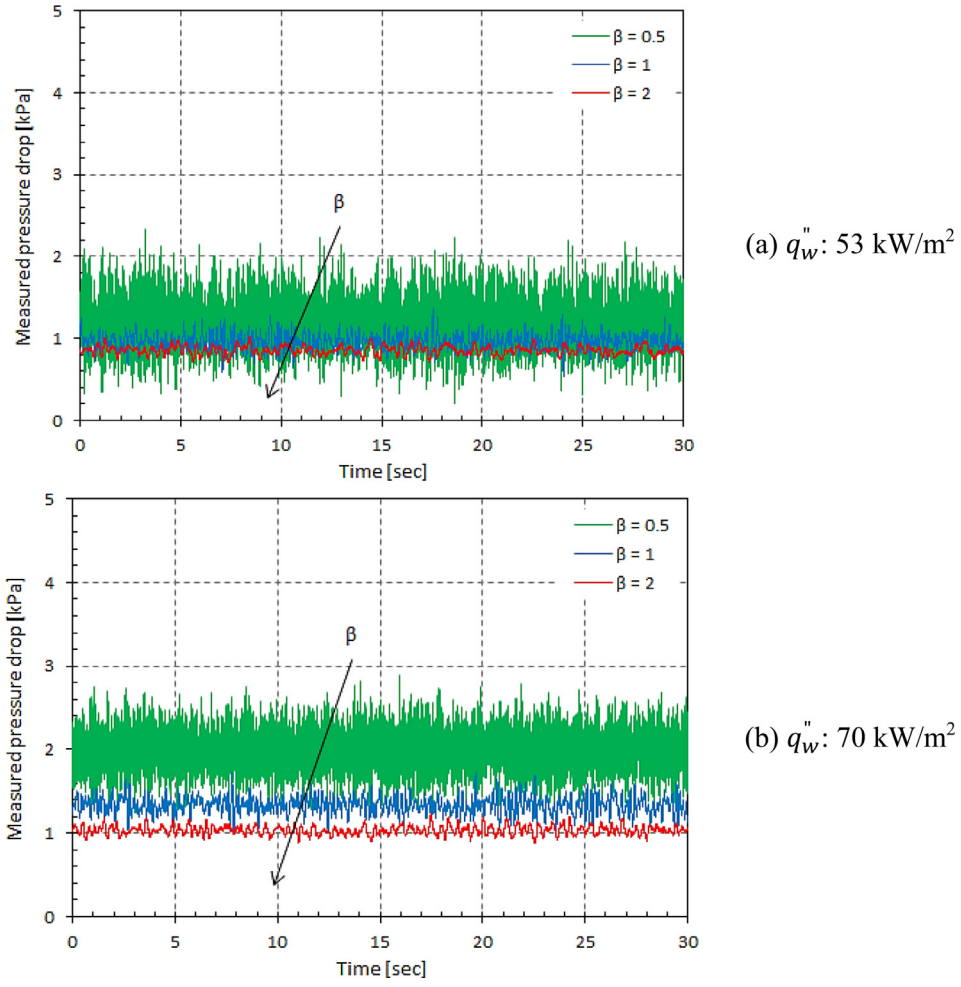

Fig. 13. Effect of aspect ratio on the measured pressure drop signal at mass flux of 150 kg/m^{2}s and two different wall heat fluxes. (For interpretation of the references to colour in this figure legend, the reader is referred to the web version of this article.)

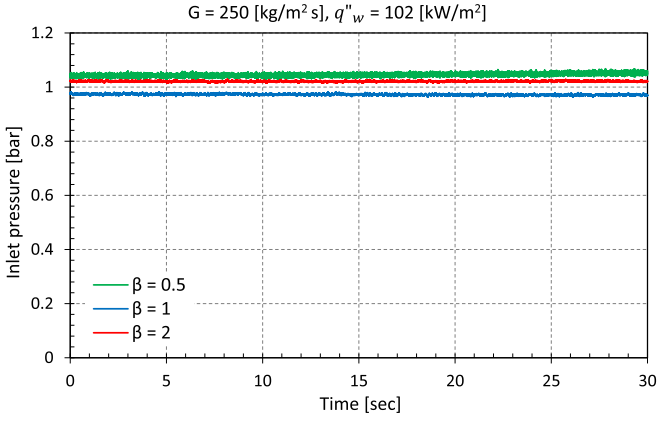

Fig. 14. Inlet pressure fluctuations at wall heat flux of 102 kW/m^2 and mass flux of 250 kg/m^{2}s for three heat sinks.

fluctuation in the measured signals for the aspect ratio of 2. Additionally, Fig. 13a indicates that at low heat fluxes the fluctuations in pressure drop was about 20% for the heat sink with the largest aspect ratio and increased to about 80% for the heat sink with smallest aspect ratio. The high fluctuations at low heat fluxes may be due to the dominance of elongated slug flow along a significant length of the channel that can expand in both directions as discussed above. These fluctuations decreased with the increase of heat flux (when bubbly/slug flow becomes limited to a short length near the entry region and annular flow dominates along the channel length). For example, Fig. 13b indicates that the pressure drop fluctuations decreased to about 40% when the heat flux increased to 70 kW/m^2.

5.4. Heat transfer characteristics

The effect of heat flux, mass flux and vapour quality on the local and average heat transfer coefficient was discussed in detail in Al-Zaidi et al. [28]. The heat transfer coefficient was found to increase with increasing wall heat flux. This was attributed to the high bubble generation and, to a lesser extent to the contribution of nucleation in the liquid film, as well as liquid film evaporation. In contrast, there was no clear mass flux effect in the examined range of 50–250 kg/m^{2}s. Moreover, the local heat transfer coefficient reached higher value at very low vapour quality and then decreased with increasing local vapour quality, see Fig. 15. It is worth mentioning that due to the short length of the channels, only three thermocouples were used for the local temperature measurements. Thus, the data in Fig. 15 were for three axial locations, i.e. z/L of 0.1, 0.5 and 0.9. This reduction in local heat transfer rates after the nucleate boiling region could be due to the development of slug, churn and later annular flow where heat transfer rates could be lower, see Lee et al. [29]. It is worth mentioning that the above results were found for all test sections. The reduction in two-phase heat transfer coefficient with vapour qualities was also

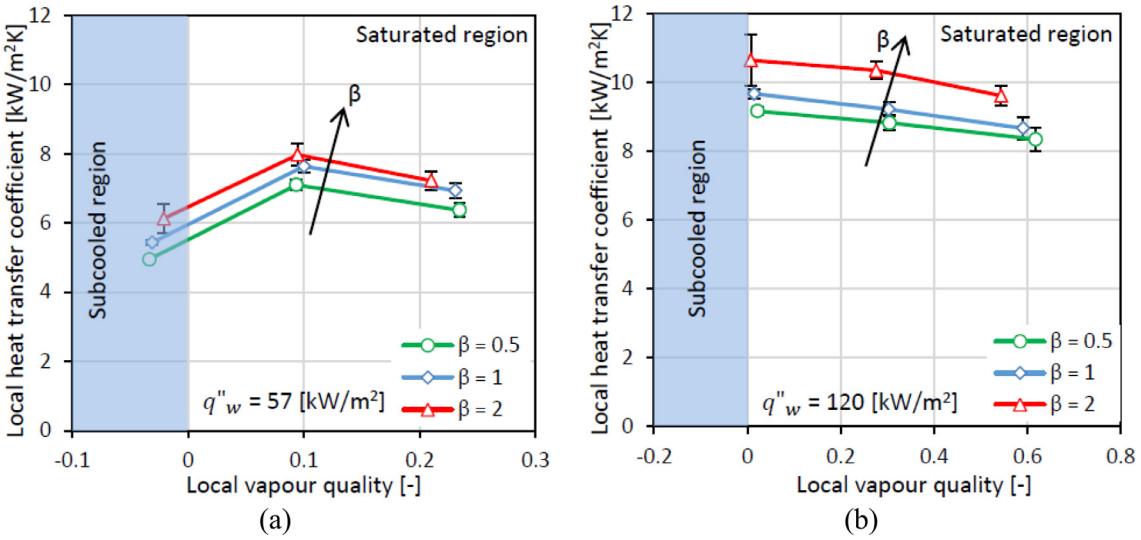

Fig. 15. Effect of channel aspect ratio on the local heat transfer coefficient at mass flux of 250 kg/m^{2}s and: (a) Low wall heat flux (b) High wall heat flux.

reported in the literature, see Qu and Mudawar [30], Steinke and Kandlikar [31], Diaz and Schmidt [32], Lee and Mudawar [33] and Korniliou and Karayiannis [34]. Qu and Mudawar [30] conducted an experimental flow boiling study using de-ionized water in horizontal rectangular microchannels with channel height and width of 0.713 and 0.231 mm, respectively. In another study by Lee and Mudawar [33], flow boiling of R134a in horizontal square channels having 1 × 1 mm dimension was investigated. This reduction was attributed by [33] to the droplet entrainment and deposition during annular flow leading to thicker film thickness. Steinke and Kandlikar [31] also conducted flow boiling experiments using water in horizontal parallel microchannels having 0.2 mm channel height and 0.214 mm channel width. They reported that very high heat transfer coefficient was reached at low vapour qualities due to the onset of nucleate boiling. After that, a reduction in the heat transfer coefficient with increasing quality was found. This was attributed by the authors to the rapid bubble growth resulting in flow reversal. Diaz and Schmidt [32] performed flow boiling of n-hexane in a horizontal rectangular channel with height and width of 0.3 mm and 12.7 mm, respectively. Their results showed that the heat transfer coefficient became high around vapour quality of zero, and then decreased rapidly with increasing quality. Korniliou and Karayiannis [34] also reported that the two-phase heat transfer coefficient decreased with local quality, using de-ionized water in a horizontal microchannel with 1 mm height and width 1 mm.

Fig. 15 illustrates the effect of channel aspect ratio on the local heat transfer coefficient at mass flux of 250 kg/m^{2}s and different wall heat fluxes. This figure demonstrates that, in the subcooled region, the local heat transfer coefficient increased with aspect ratio. This could be due to the lower wall temperature as a result of the wider channel width. In the saturation region, there was a noticeable increase in the local heat transfer coefficient when the channel aspect ratio increased. This aspect ratio effect became clear at high wall heat flux as shown in Fig. 15(b). The channel aspect ratio may affect the bubble nucleation site density and the liquid film thickness as shown schematically in Fig 16. At low vapour qualities when the flow pattern is bubbly flow, the enhancement in the heat transfer coefficient with the increase in aspect ratio could be due to the activation of more nucleation sites at the channel corners and on the channel bottom surface due to the large channel width, see Fig 16(a). When the channel width decreases, bubble nucleation may only be limited to the channel corners. In other words, the number of nucleation sites is larger in the channel with a larger bottom surface area. It is known that more nucleation sites result in higher heat transfer coefficient due to the evaporation process in the liquid micro-layer underneath these nucleating bubbles. At moderate and high vapour qualities, when the flow pattern is slug or annular flow, the difference in the heat transfer coefficient with different aspect ratios could be due to the behaviour and distribution of the liquid film around the channel circumference as explained schematically in Fig 16(b) and discussed by Magnini and Matar [22]. In the shallow channel, i.e. large aspect ratio, the slug or annular flow is confined and squeezed between the channel bottom surface and the top adiabatic surface leaving a thin liquid film. Since the channels are heated from the bottom surface (partial heated channel), the evaporation rate is expected to be very high at the liquid film interface in contact with the bottom surface. Also, the thicker film and high superheat at the side walls in shallow channels as reported by Magnini and Mater [22] could help bubble nucleation in the liquid film. In contrast, in the deep channel, i.e. small aspect ratio, these flow patterns are confined and squeezed by the channel sidewalls rather than the channel bottom surface. Therefore, the liquid film thickness may become thicker on the channel bottom surface. This leads to increase the thermal resistance and decrease the evaporation rate leading to lower heat transfer coefficient.

Fig. 17 presents the average heat transfer coefficient at three channel aspect ratios and mass flux of 250 kg/m^{2}s. This figure illustrates that the average heat transfer coefficient increased with increasing wall heat flux. It also shows that when the channel aspect ratio increased from 0.5 to 2, the average heat transfer coefficient increased by 14.3% for the heat flux range studied. The increase in the two-phase heat transfer coefficient with channel aspect ratio was also reported by other researchers, such as Soupremanien et al. [11] (at low heat fluxes), Markal et al. [13] (up to aspect ratio of 3.54) and Drummond et al. [35].

Fig. 18 depicts the effect of channel aspect ratio on the boiling curve at mass flux of 250 kg/m^{2}s. Both wall and base heat fluxes were plotted here to discuss the effect of aspect ratio. Generally, the wall superheat (wall-to-saturation temperature difference) increased with increasing wall or base heat flux for all test sections. Fig. 18(a) shows that, for a fixed wall superheat, the wall heat flux increased by 22.3% (average difference) when the channel aspect ratio increased from 0.5 to 2. In other words, when the wall heat flux is the required parameter, a noticeable influence of aspect ratio on the boiling curve was found. From a design point of view,

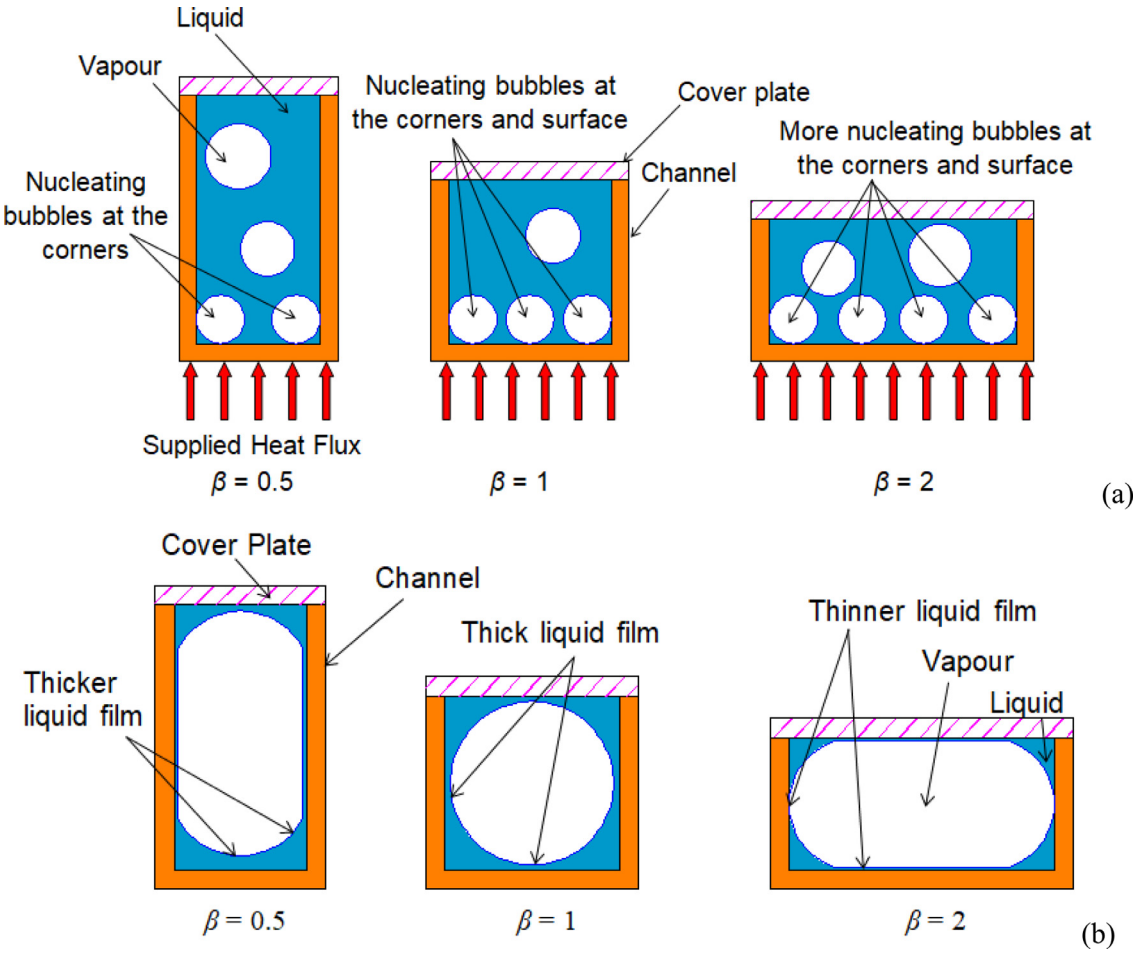

Fig. 16. Schematic diagram of the aspect ratio effect on the: (a) Nucleation site density (b) Liquid film thickness around the channel circumference.

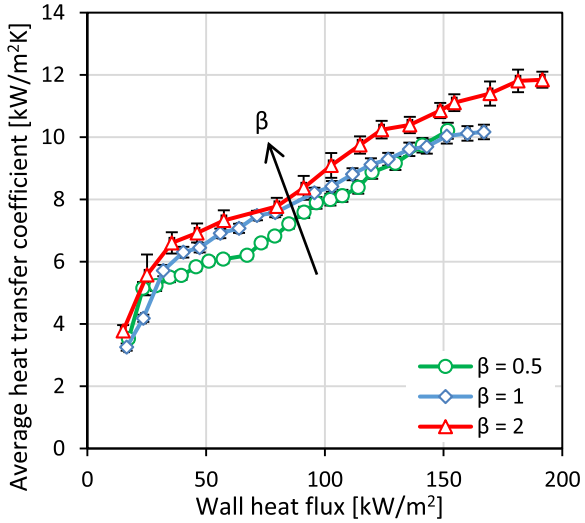

Fig. 17. Average heat transfer coeffecnet at different aspect ratios and mass flux of 250 kg/m^{2}s.

the dissipated heat from any chipset should be considered when a thermal management system is proposed for electronics cooling. Accordingly, the boiling curve was plotted using the base heat flux versus wall superheat as shown in Fig. 18(b). It is obvious that when the channel aspect ratio decreased, the base heat flux was found to increase and also the slope of the boiling curve increased. This opposite trend of aspect ratio with base heat flux compared to wall heat flux could be attributed to the effect of surface area ratio. The surface area ratio can be defined as a ratio between the total heat transfer area and the base area as presented in Eq. (26).

$$\alpha = \frac{(2H_{ch} + W_{ch})N}{W_b} \tag{26}$$

The total heat transfer area, (and hence the area ratio) differs from heat sink to another since the channel dimensions and the number of channels are not the same. Therefore, the area ratio increases with decreasing channel aspect ratio leading to an increase in the base heat flux as shown in Eq. (27).

$$q_b'' = q_w'' * \alpha \tag{27}$$

In other words, the maximum heat that can be dissipated from the chipset increases with decreasing aspect ratio due to the large surface enhancement. This can outweigh the benefits from the boiling heat transfer enhancement at larger channel aspect ratio. Fig. 18(b) depicts that maximum base heat flux reached up to 531.2, 414.8 and 335.3 kW/m^2, when the aspect ratio was 0.5, 1 and 2, respectively, which corresponds to the cooling load of 265.6, 207.4 and 167.6 W, respectively for a base area of 20 mm × 25 mm.

5.5. Pressure drop characteristics

Pressure drop is considered an important parameter that defines the pump performance and energy use. This component may be affected by the channel aspect ratio. Therefore, the influence

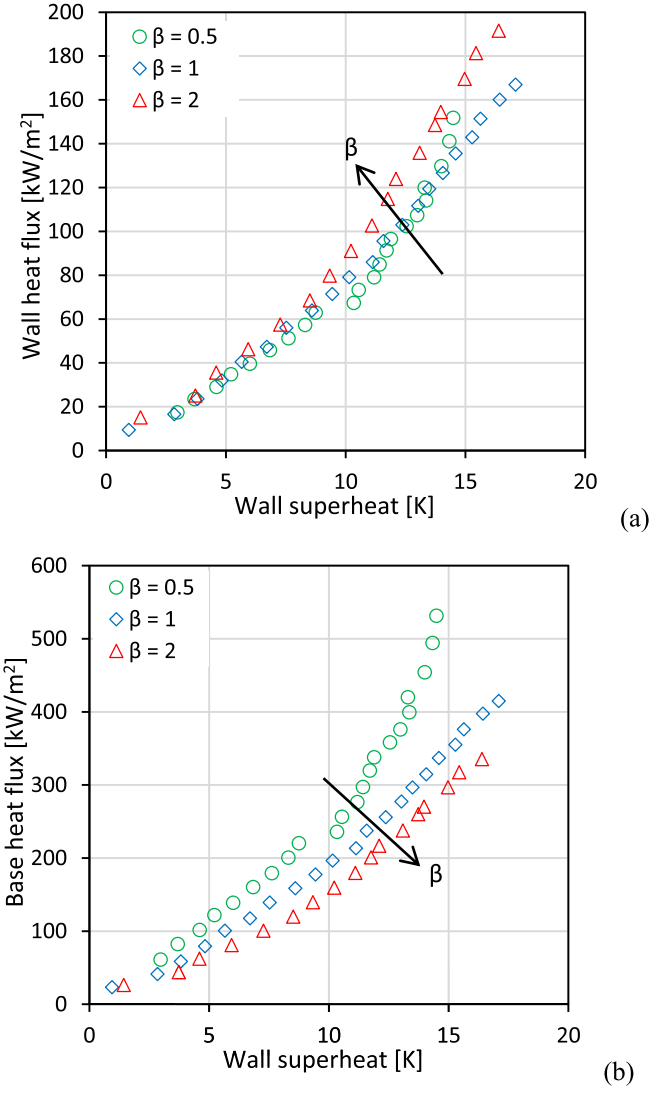

Fig. 18. Apsect ratio effect on the boiling curve at mass flux of 250 kg/m^{2}s and z/L of 0.5: (a) Wall heat flux (b) Base heat flux.

of aspect ratio on the flow boiling pressure drop at mass flux of 250 kg/m^{2}s is presented in Fig. 19. This figure shows that, for all channel aspect ratios, the flow boiling pressure drop increased with wall heat flux. This could be due to the high bubble generation and thus high flow resistance leading to an increase in the flow boiling pressure drop. The increase in flow boiling pressure drop with heat flux (or exit quality) was also reported by Qu and Mudawar [36], Harirchian and Garimella [5], Huang et al. [37] and Markal et al. [38]. This figure also illustrates that, for a given wall heat flux, the flow boiling pressure drop increased with deceasing channel aspect ratio. The effect of aspect ratio became noticeable at moderate and high heat fluxes, i.e. more than 60 kW/m^2, when a higher bubble generation occurred and annular flow dominated. The flow boiling pressure drop was found to increase by 48.6% (average difference) when the aspect ratio decreased from the larger to smaller value. The maximum flow boiling pressure drop reached in these experiments was 3.98, 5.5 and 5.6 kPa, when the aspect ratio was 2, 1 and 0.5, respectively. Using the corresponding mass flow rates, the increase in the energy consumed by the pump (volume flow rate × measured pressure drop) is 9.7 mW, which is small compared to the total pressure drop in a thermal management system. It is worth mentioning that other researchers also

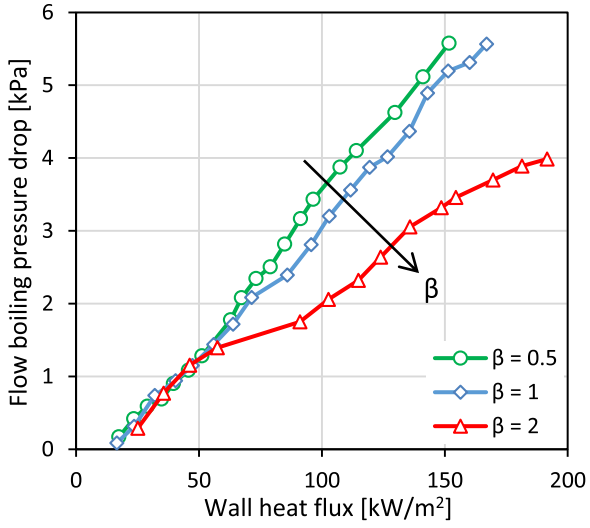

Fig. 19. Effect of channel aspect ratio on the flow boiling pressure drop at mass flux of 250 kg/m^{2}s.

found that the flow boiling pressure drop varied inversely proportional to the channel aspect ratio or increased as the channel height increased (at a fixed width) or channel width decreased (at a fixed height), see Harirchian and Garimella [5], Holcomb et al. [8], Soupremanien et al. [11], Drummond et al. [35] and Özdemir [39]. This effect of channel aspect ratio on the pressure drop could be attributed to: (1) The difference in the exit vapour quality due to the different heat transfer areas. For a fixed wall heat flux, the channel aspect ratio of 0.5 has the largest heat transfer area compared to the aspect ratio of 2. This results in higher heat transfer rate and thus higher exit vapour quality, i.e. higher void fraction. (2) The difference in the distribution of the liquid film. During annular flow, for the deeper channels (smaller aspect ratio) the liquid film at the channel bottom surface is expected to be thicker due to stratification effects, see Fig. 16(b). In contrast, for the shallow channels, i.e. larger aspect ratio, most of the liquid may collect at the channel corners leaving a very thin liquid film at the channel bottom surface and sidewalls. Therefore, the wall shear stress (between liquid film and channel surface) at the channel bottom in addition to the channel sidewalls is expected to be larger compared to the shallow channels. This may result in larger frictional pressure drop component in the deeper channels.

6. Conclusions

Flow boiling experiments of HFE-7100 in horizontal multi-microchannel heat sinks were carried out. Three different channel aspect ratios, i.e. 0.5, 1.0 and 2.0, at hydraulic diameter of 0.46 mm were tested. The experiments were set at mass flux ranging from 50 to 250 kg/m^{2}s, wall heat flux range from 9.6 to 191.6 kW/m^2, system pressure of 1 bar (measured at the test section inlet) and inlet sub-cooling near 5 K. The main conclusions can be summarised as follows:

1. The observed flow patterns were bubbly, slug, churn and annular flow. Small nucleating bubbles in the liquid film of annular flow were also visualized.
2. Flow reversal occurred in all experiments. The cycle of flow reversal was found to be forward motion, stagnation period and backward motion, while the captured flow regimes were fluctuating between bubbly, confined bubble and slug flow. This flow reversal resulted in fluctuations in pressure drop, which were higher in the channels with small aspect ratio, especially at low heat fluxes. However, this mild flow reversal and fluctuations

in pressure drop did not affect the heat transfer results significantly.

3. The bubble size was found to increase with decreasing aspect ratio. This could be due to the confinement effect and heat transfer from the side walls. Slug ends became more round with deceasing aspect ratio, while there was no a clear effect on annular flow.
4. The heat transfer results demonstrated that the heat transfer coefficient reached higher values at very low vapour qualities then decreased with further quality increases. Moreover, it was found to increase with wall heat flux, while there was insignificant effect of mass flux.
5. A small enhancement in the heat transfer coefficient was found with increasing channel aspect ratio. Compared to the aspect ratio of 0.5, the average heat transfer coefficient increased by 14.3% for an aspect ratio of 2.
6. The flow boiling pressure drop results showed that the pressure drop increased with increasing wall heat flux while it decreased with increasing aspect ratio.
7. The maximum heat that can be dissipated from the chipset (base heat flux) increased with decreasing channel aspect ratio. This is due to the large surface area enhancement, which outweighs the increase in the heat transfer coefficient.
8. The present study demonstrated that, the channel aspect ratio has a significant effect on both base heat flux and pressure drop. Accordingly, this parameter should be considered in any proposed small to micro-scale thermal management system. However, more experimental work is required to confirm this by testing different aspect ratio ranges, operating conditions and working fluids.
9. The maximum base heat flux reached in this study was 530 kW/m^2, i.e. cooling load of 265 W, using the smaller channel aspect ratio. The working surface temperature can be controlled to be less than 80°C, allowing such systems to be used in cooling of electronics.

Author statement

Tassos G. Karayiannis planned the project. Mohamed Mahmoud designed and constructed the original experimental facility under the supervision of T.G. Karayiannis. Ali H Al-Zaidi, supervised by both M. Mahmoud and T.G. Karayiannis, modified the experimental facility and carried out the present experiments and analysis of results. Ali H. Al-Zaidi presented the results and first draft for changes and additions to the other two authors. All authors discussed the results and contributed to the final manuscript.

Declaration of Competing Interest

The authors declare that they have no known competing financial interests or personal relationships that could have appeared to influence the work reported in this paper.

Acknowledgements

Ali Al-Zaidi would like to thank the Iraqi Ministry of Higher Education and Scientific Research (MOHESR) for their financial support for his PhD studies at Brunel University London.

Supplementary materials

Supplementary material associated with this article can be found, in the online version, at doi:10.1016/j.ijheatmasstransfer.2020.120587.

References

[1] T.G. Karayiannis, M.M. Mahmoud, Flow boiling in microchannels: fundamentals and applications, Appl. Therm. Eng. 115 (2017) 1372–1397.
[2] L. Cheng, G. Xia, Fundamental issues, mechanisms and models of flow boiling heat transfer in microscale channels, Int. J. Heat Mass Transf. 108 (2017) 97–127.
[3] Chapter 4 M.M. Mahmoud, T.G. Karayiannis, Flow Boiling in Mini to Micro Diameter Channels, in: John R. Thome (Ed.), Encyclopaedia of Two-Phase Heat Transfer and Flow IV World Scientific Publishers, 2018. Chapter 4Ed. https://doi.org/10.1142/9789813234444_0004 .
[4] S.G. Singh, A. Kulkarni, S.P. Duttagupta, B.P. Puranik, A. Agrawal, Impact of aspect ratio on flow boiling of water in rectangular microchannels, Exp. Therm. Fluid Sci. 33 (1) (2008) 153–160.
[5] T. Harirchian, S.V. Garimella, Microchannel size effects on local flow boiling heat transfer to a dielectric fluid, Int. J. Heat Mass Transf. 51 (15–16) (2008) 3724–3735.
[6] T. Harirchian, S.V. Garimella, Effects of channel dimension, heat flux, and mass flux on flow boiling regimes in microchannels, Int. J. Multiph. Flow 35 (4) (2009) 349–362.
[7] T. Harirchian, S.V. Garimella, The critical role of channel cross-sectional area in microchannel flow boiling heat transfer, Int. J. Multiph. Flow 35 (10) (2009) 904–913.
[8] B.T. Holcomb, T. Harirchian, S.V. G.arimella, An Experimental Investigation of Microchannel Size Effects on Flow Boiling With De-Ionized Water, in: Proceedings of the ASME 2009 Heat Transfer Summer Conference, 2009, pp. 1–9.
[9] C.W. Choi, D.I. Yu, M.H. Kim, Adiabatic two-phase flow in rectangular microchannels with different aspect ratios: part I - Flow pattern, pressure drop and void fraction, Int. J. Heat Mass Transf. 54 (1–3) (2011) 616–624.
[10] C.W. Choi, D.I. Yu, M.H. Kim, Adiabatic two-phase flow in rectangular microchannels with different aspect ratios: part II - Bubble behaviors and pressure drop in single bubble, Int. J. Heat Mass Transf. 53 (23–24) (2010) 5242–5249.
[11] U. Soupremanien, S. Le Person, M. Favre-Marinet, Y. Bultel, Influence of the aspect ratio on boiling flows in rectangular mini-channels, Exp. Therm. Fluid Sci. 35 (2011) 797–809.
[12] B.-.R. Fu, C.-.Y. Lee, C. Pan, The effect of aspect ratio on flow boiling heat transfer of HFE-7100 in a microchannel heat sink, Int. J. Heat Mass Transf. 58 (1–2) (2013) 53–61.
[13] B. Markal, O. Aydin, M. Avci, Effect of aspect ratio on saturated flow boiling in microchannels, Int. J. Heat Mass Transf. 93 (2016) 130–143.
[14] M.R. Özdemir, M.M. Mahmoud, T.G. Karayiannis, Flow Boiling of Water in a Rectangular Metallic Microchannel, Heat Transf. Eng. (2020) 1–25.
[15] R. Remsburg, Thermal design of electronic equipment, 2001.
[16] R.K. Shah, A.L. London, Laminar Flow Forced Convection in ducts, Supplement 1 to Advances in Heat Transfer, Academic Press, New York, 1978.
[17] H.W. Coleman, W.G. Steele, Experimentation and Uncertainty Analysis For Engineers, 3nd ed, Wiley, Chichester, New York, 2009.
[18] L.C. Hsu, S.W. Cion, K.W. Lin, C.C. Wang, An experimental study of inclination on the boiling heat transfer characteristics of a micro-channel heat sink using HFE-7100, Int. Commun. Heat Mass Transf. 62 (2015) 13–17.
[19] A.H. Al-Zaidi, M.M. Mahmoud, T.G. Karayiannis, Condensation Flow Patterns and Heat Transfer in Horizontal Microchannels, Exp. Therm. Fluid Sci. 90 (2018) 153–173.
[20] X.F. Peng, G.P. Peterson, Convective heat transfer and flow friction for water flow in microchannel structures, Int. J. Heat Mass Transf. 39 (12) (1996) 2599–2608.
[21] M. Mirmanto, Single-phase flow and flow boiling of water in horizontal rectangular microchannels Brunel University London (PhD thesis), London, UK, 2013.
[22] M. Magnini, O.K. Matar, Numerical study of the impact of the channel shape on microchannel boiling heat transfer, Int. J. Heat Mass Transf. 150 (2020) 119322.
[23] S.G. Kandlikar, Nucleation characteristics and stability considerations during flow boiling in microchannels, Exp. Therm. Fluid Sci. 30 (5) (2006) 441–447.
[24] S.G. Kandlikar, Scale effects on flow boiling heat transfer in microchannels: a fundamental perspective, Int. J. Therm. Sci. 49 (7) (2010) 1073–1085.
[25] T. Chen, S.V. Garimella, Measurements and high-speed visualizations of flow boiling of a dielectric fluid in a silicon microchannel heat sink, Int. J. Multiph. Flow 32 (8) (2006) 957–971.
[26] K.-.S. Yang, Y.-.R. Jeng, C.-.M. Huang, C.-.C. Wang, Heat Transfer and Flow Pattern Characteristics for HFE-7100 Within Microchannel Heat Sinks, Heat Transf. Eng. 32 (7–8) (2011) 697–704.
[27] E.M. Fayyadh, M.M. Mahmoud, K. Sefiane, T.G. Karayiannis, Flow boiling heat transfer of R134a in multi microchannels, Int. J. Heat Mass Transf. 110 (2017) 422–436.
[28] A.H. Al-Zaidi, M.M. Mahmoud, T.G. Karayiannis, Flow boiling of HFE-7100 in microchannels: experimental study and comparison with correlations, Int. J. Heat Mass Transf. 140 (2019) 100–128.
[29] V.Y.S. Lee, T.G. Karayiannis, G. Henderson, Flow Boiling Heat Transfer in Plain and Coated Microchannel Heat Sinks Using HFE-7200, in: Proceedings of the ASME 2020 18th International Conference on Nanochannels, Microchannels, and Minichannels, ICNMM2020, 2020, pp. 1–10.
[30] W. Qu, I. Mudawar, Flow boiling heat transfer in two-phase micro-channel heat sinks —- II . Annular two-phase flow model, Int. J. Heat Mass Transf. 46 (2003) 2773–2784.

[31] M.E. Steinke, S.G. Kandlikar, An Experimental Investigation of Flow Boiling Characteristics of Water in Parallel Microchannels, J. Heat Transfer 126 (4) (2004) 518–526.
[32] M.C. Diaz, J. Schmidt, Flow Boiling of n-Hexane in Small Channels: heat Transfer Measurements and Flow Pattern Observations, Chem. Eng. Technol. 30 (3) (2007) 389–394.
[33] S. Lee, I. Mudawar, Enhanced model for annular flow in micro-channel heat sinks, including effects of droplet entrainment/deposition and core turbulence, Int. J. Heat Mass Transf. 133 (2019) 510–530.
[34] S. Korniliou, T.G. Karayiannis, Flow boiling of water in square cross section microchannel at different inlet subcooling conditions, in: Proceedings of the 5th World Congress on Momentum, Heat and Mass Transfer (MHMT'20), 2020.
[35] K.P. Drummond, D. Back, M.D. Sinanis, D.B. Janes, D. Peroulis, J.A. Weibel, S.V. Garimella, A hierarchical manifold microchannel heat sink array for high--heat-flux two-phase cooling of electronics, Int. J. Heat Mass Transf. 117 (2018) 319–330.
[36] W. Qu, I. Mudawar, Transport Phenomena in Two-Phase Micro-Channel Heat Sinks, J. Electron. Packag. 126 (2004) 213–224.
[37] H. Huang, N. Borhani, J.R. Thome, Experimental investigation on flow boiling pressure drop and heat transfer of R1233zd(E) in a multi-microchannel evaporator, Int. J. Heat Mass Transf. 98 (2016) 596–610.
[38] B. Markal, O. Aydin, M. Avci, An experimental investigation of saturated flow boiling heat transfer and pressure drop in square microchannels, Int. J. Refrig. 65 (2016) 1–11.
[39] M.R. Özdemir, Single – Phase Flow and Flow Boiling of Water in Rectangular Metallic Microchannels Brunel University London (PhD thesis), London, UK, 2016.